

RESEARCH ARTICLE SUMMARY

ENDOCRINOLOGY

Artemisinins ameliorate polycystic ovarian syndrome by mediating LONP1-CYP11A1 interaction

Yang Liu[†], Jing-jing Jiang[†], Shao-yue Du[†], Liang-shan Mu, Jian-jun Fan, Jun-chi Hu, Yao Ye, Meng Ding, Wei-yu Zhou, Qiu-han Yu, Yi-fan Xia, Hong-yu Xu, Yi-jie Shi, Shu-wen Qian, Yan Tang, Wei Li, Yong-jun Dang, Xi Dong, Xiao-ying Li, Cong-jian Xu, Qi-qun Tang*

INTRODUCTION: Polycystic ovarian syndrome (PCOS), a prevalent reproductive endocrine disorder affecting 10 to 13% of women in their reproductive age, is characterized by hyperandrogenemia, ovulatory dysfunction, polycystic ovarian morphology, and often by associated metabolic disorders. Androgen excess is a key factor driving the phenotypic features of PCOS. Despite the high prevalence of PCOS, pharmacologic interventions for such a complicated syndrome encounter substantial challenges. The treatment options currently available for PCOS are limited and mainly tailored to management of specific symptoms. Consequently, there is a compelling and urgent need for the development of innovative therapeutic strategies.

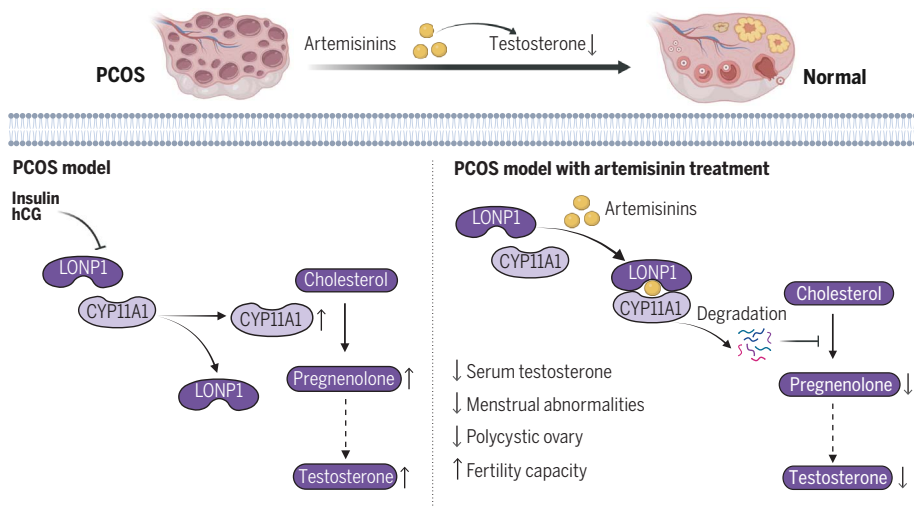
RATIONALE: Artemisinin, derived from *Artemisia* plants, is widely recognized for its efficacy against malaria. We have previously demonstrated that artemisinin and its derivatives possess the capability to enhance energy ex-

penditure and insulin sensitivity through the activation of thermogenic adipocytes, thereby protecting against diet-induced obesity and metabolic disorders. In this study, we explored the therapeutic potential of artemisinins in rodent PCOS-like models and human patients with PCOS by evaluating the effect of artemisinin derivatives on testosterone level, estrous cycle, and polycystic ovarian morphology. Using *in vitro* and *in vivo* approaches, we investigated the impact of artemisinins on ovarian testosterone synthesis. The direct target of artemisinins was identified to elucidate the mechanism governing the regulation of testosterone synthesis by artemisinins.

RESULTS: We found that artemisinin analog artemether exhibited considerable improvements in hyperandrogenemia, irregular estrous cycles, polycystic ovarian morphology, and low fertility in the PCOS-like rodent models. Artemisinins inhibited hyperandrogenemia by repressing

ovarian testosterone synthesis. Relative quantitative proteomics analysis revealed cytochrome P450 family 11 subfamily A member 1 (CYP11A1), the enzyme catalyzing the initial step of androgen synthesis, as the most notably decreased protein affected by artemisinins. Further investigation showed that artemisinins induced the degradation of CYP11A1, leading to the inhibition of ovarian androgen synthesis. This inhibitory effect was diminished in the absence of CYP11A1. Mechanistically, artemisinins directly targeted the Lon peptidase 1 (LONP1), enhancing the interaction between LONP1 and CYP11A1 and promoting the LONP1-catalyzed degradation of CYP11A1. Conversely, androgenic inducer disrupted the binding between LONP1 and CYP11A1; additionally, LONP1 was down-regulated in PCOS, resulting in elevated CYP11A1 levels and increased androgen synthesis. Protein-docking simulations and subsequent functional experiments suggested that the inhibitory effect of artemisinins on CYP11A1 level largely depended on their direct binding to the proteolytic domain of LONP1. Consistent with the function of artemisinins, LONP1 overexpression strongly suppressed androgen production in the ovary. Lastly, a pilot clinical trial was conducted to confirm the therapeutic effects of artemisinins in patients with PCOS. We found that dihydroartemisinin treatment effectively ameliorated hyperandrogenemia, reduced anti-Müllerian hormone levels, improved polycystic ovarian morphology, and contributed to the normalization of menstruation in patients with PCOS.

CONCLUSION: Our data demonstrated the efficacy of artemisinins in alleviating symptoms associated with PCOS in both rodent models and human patients. Artemisinins directly bind to LONP1, initiating the interaction between LONP1 and CYP11A1, which in turn promotes the degradation of CYP11A1, subsequently inhibiting ovarian androgen synthesis and curbing PCOS. Contrarily, androgenic inducer disrupts LONP1-CYP11A1 interaction and aggravates PCOS. Overall, our findings highlight the promising potential of artemisinins as effective drugs for the comprehensive treatment of PCOS. This discovery illuminates a previously unknown interaction between LONP1 and CYP11A1 that is enhanced by artemisinins to govern androgen synthesis, opening avenues for PCOS intervention by targeting LONP1-CYP11A1 interaction. ■



Artemisinins inhibit ovarian androgen synthesis and relieve PCOS. The pro-androgen inducer human chorionic gonadotropin (hCG) disrupts the interaction between LONP1 and CYP11A1, leading to the up-regulation of CYP11A1, which promotes androgen production and exacerbates PCOS. Conversely, artemisinins mediate LONP1-CYP11A1 interaction, promoting the degradation of CYP11A1 and subsequently inhibiting ovarian androgen synthesis. Consequently, artemisinins show efficacy in ameliorating PCOS symptoms in both rodents and human patients [Figure created with BioRender.com].

The list of author affiliations is available in the full article online.

*Corresponding author. Email: qqtang@shmu.edu.cn

†These authors contributed equally to this work.

Cite this article as Y. Liu et al., *Science* **384**, eadk5382 (2024). DOI: 10.1126/science.adk5382

S READ THE FULL ARTICLE AT
<https://doi.org/10.1126/science.adk5382>

RESEARCH ARTICLE

ENDOCRINOLOGY

Artemisinins ameliorate polycystic ovarian syndrome by mediating LONP1-CYP11A1 interaction

Yang Liu^{1†}, Jing-jing Jiang^{1†}, Shao-yue Du^{2†}, Liang-shan Mu³, Jian-jun Fan⁴, Jun-chi Hu⁴, Yao Ye³, Meng Ding¹, Wei-yu Zhou¹, Qiu-han Yu⁵, Yi-fan Xia¹, Hong-yu Xu¹, Yi-jie Shi¹, Shu-wen Qian¹, Yan Tang¹, Wei Li⁵, Yong-jun Dang⁴, Xi Dong³, Xiao-ying Li¹, Cong-jian Xu², Qi-qun Tang^{1*}

Polycystic ovary syndrome (PCOS), a prevalent reproductive disorder in women of reproductive age, features androgen excess, ovulatory dysfunction, and polycystic ovaries. Despite its high prevalence, specific pharmacologic intervention for PCOS is challenging. In this study, we identified artemisinins as anti-PCOS agents. Our finding demonstrated the efficacy of artemisinin derivatives in alleviating PCOS symptoms in both rodent models and human patients, curbing hyperandrogenemia through suppression of ovarian androgen synthesis. Artemisinins promoted cytochrome P450 family 11 subfamily A member 1 (CYP11A1) protein degradation to block androgen overproduction. Mechanistically, artemisinins directly targeted Lon peptidase 1 (LONP1), enhanced LONP1-CYP11A1 interaction, and facilitated LONP1-catalyzed CYP11A1 degradation. Overexpression of LONP1 replicated the androgen-lowering effect of artemisinins. Our data suggest that artemisinin application is a promising approach for treating PCOS and highlight the crucial role of the LONP1-CYP11A1 interaction in controlling hyperandrogenism and PCOS occurrence.

Polyzystic ovarian syndrome (PCOS) is a complicated reproductive-metabolic disease and one of the most common endocrine disorders affecting women of reproductive age, with a prevalence of 10 to 13% (1–4). It encompasses diverse clinical symptoms, including hyperandrogenism, oligoovulation or anovulation, polycystic ovaries, and in many cases, metabolic disorders (5–8). Androgen excess is the main driver of numerous phenotypic features of PCOS, such as follicular dysplasia, impaired ovulation, endometrial diseases, and metabolic dysfunction (9). In addition, prenatal androgen exposure induces PCOS-like traits in female offspring, heightening the transgenerational susceptibility to PCOS (10). Consequently, controlling androgen excess is crucial to PCOS intervention.

In women, androgens are primarily synthesized by the adrenal glands and ovaries. These hormones are derived from cholesterol through

a series of enzymatic reactions catalyzed by cytochromes P450 (CYP) and hydroxysteroid dehydrogenase (HSD), including CYP family 11 subfamily A member 1 (CYP11A1), CYP17A1, HSD3B2, and HSD17B (11, 12). Within the ovary, androstenedione and testosterone are predominantly synthesized in ovarian theca cells and diffuse into granulosa cells, where they are converted into estrogen by aromatase (CYP19A1) (11). Ovarian steroidogenesis is highly responsive to androgenic stimuli such as luteinizing hormone (LH) or human chorionic gonadotropin (hCG). Numerous studies have demonstrated an increase in the expression of CYP11A1 and CYP17A1, as well as elevated enzyme activity of CYP17A1, HSD3B, and HSD17B in the ovarian theca cells of PCOS, resulting in elevated production of progesterone, 17 α -hydroxyprogesterone (17 α -OHP), and testosterone (13–16). Therefore, inhibiting the excessive expression of these steroidogenesis-related enzymes may be effective for controlling hyperandrogenemia and PCOS.

Currently, pharmacologic interventions for PCOS are mainly tailored to management of specific symptoms. Few available drugs effectively target all aspects of PCOS. Combined oral contraceptives (COCs) are recommended for managing hyperandrogenism and/or irregular menstrual cycles in adult women with PCOS. However, COCs do not improve infertility and polycystic ovary morphology. Moreover, COCs are often associated with side effects such as vascular thromboembolism (17), which limit their long-term clinical application, particularly for PCOS patients with metabolic disorders. Artemisinin, a molecule

isolated from *Artemisia* plants, exerts an anti-malarial effect (18). We have previously demonstrated that artemisinin and its derivatives, including artemether (ATM), artesunate (ATS), and SM934, can promote energy expenditures and insulin sensitivity by activating thermogenic adipocytes (19), thereby protecting against high-fat diet-induced obesity and metabolic disorders. In this study, artemisinins were identified as promising candidates for treating PCOS because they strongly inhibited ovarian androgen synthesis, reduced immature follicles, and improved the estrous cycle in both PCOS rodent models and patients.

Results

ATM exerts an inhibitory effect against PCOS-like phenotype in rodent models

To evaluate the effect of artemisinins on PCOS development, we established a PCOS-like mouse model using dehydroepiandrosterone (DHEA) and simultaneously treated the mice with ATM, a type of artemisinin (Fig. 1, A and B). When administered simultaneously, ATM ablated the elevated serum testosterone in DHEA-treated mice, thereby preventing PCOS-like traits (Fig. 1C). The disrupted estrous cycle caused by DHEA was improved by ATM (Fig. 1D). Ovaries from PCOS-like mice exhibited increased numbers of cyst-like follicles and antral follicles and decreased postovulation corpus luteum, whereas the ovaries of ATM-treated mice showed normal morphology with ovarian follicles at different stages of development (Fig. 1E). Metabolic measurements revealed that ATM had no effect on body weight, fat mass, lean mass, hepatic steatosis, and glucose tolerance (fig. S1, A to D). ATM demonstrated an improvement trend in insulin sensitivity in DHEA-treated mice (fig. S1E), which is one of the indicators for PCOS alleviation (3), although there was no statistical difference. ATM reduced serum triglyceride (TG) in DHEA-induced mice (fig. S1F) but had no effect on total cholesterol (TC) and glucose levels (fig. S1, G and H). Additionally, ATM was safe, with no liver toxicity as indicated by unchanged alanine aminotransferase (ALT) and aspartate aminotransferase (AST) levels (fig. S1I).

Building upon the observed preventive effect, the therapeutic effects of ATM were assessed. After establishment of a DHEA-induced PCOS-like model, mice were treated with varying dosages of ATM through intraperitoneal injections (Fig. 1F). ATM dose-dependently decreased serum testosterone (Fig. 1G), recovered normal estrous cycles (Fig. 1H), inhibited uterus edema (Fig. 1I), and dramatically reduced cystic follicles in the ovaries (Fig. 1J). Comparable therapeutic effects were observed upon oral administration of ATM (Fig. 1, K to O).

Next, we investigated the anti-PCOS effect of ATM in a rat model (Fig. 2A). Intraperitoneal injection of 15 mg/kg ATM sufficed to

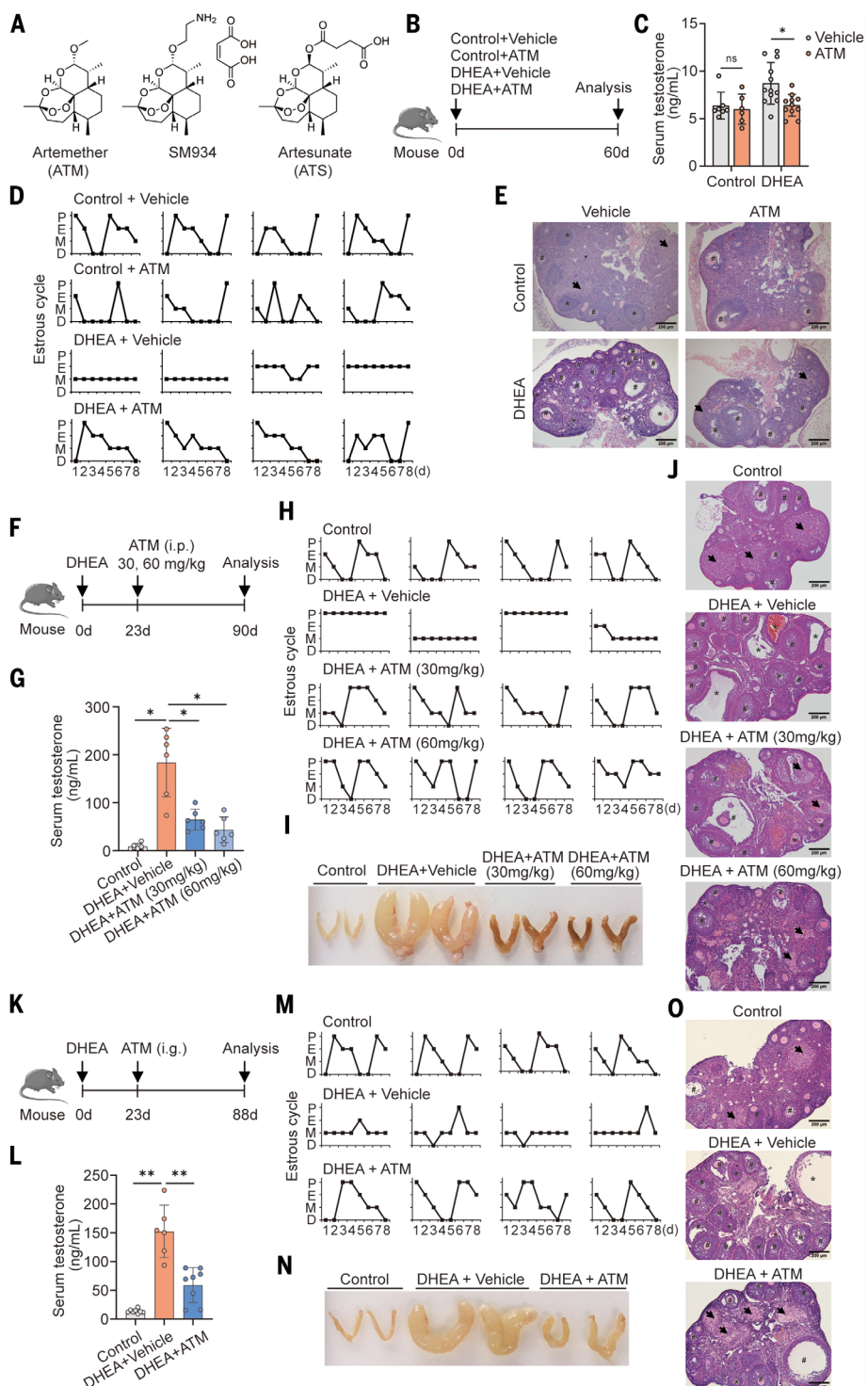
¹Key Laboratory of Metabolism and Molecular Medicine of the Ministry of Education, Department of Biochemistry and Molecular Biology of School of Basic Medical Sciences and Department of Endocrinology and Metabolism of Zhongshan Hospital, Fudan University, Shanghai 200032, China.

²Shanghai Key Laboratory of Female Reproductive Endocrine Related Disease, Obstetrics and Gynecology Hospital, Fudan University, Shanghai 200032, China. ³Reproductive Medicine Center, Zhongshan Hospital, Fudan University, Shanghai 200032, China. ⁴Basic Medicine Research and Innovation Center for Novel Target and Therapeutic Intervention, Ministry of Education, Institute of Life Sciences, the Second Affiliated Hospital of Chongqing Medical University, Chongqing 400010, China. ⁵Department of Medicinal Chemistry, School of Pharmacy, China Pharmaceutical University, Nanjing, Jiangsu 211198, China.

*Corresponding author. Email: qqtang@shmu.edu.cn

†These authors contributed equally to this work.

Fig. 1. Identification of ATM as an anti-PCOS agent in mouse model. (A) Chemical structures of artemether (ATM), SM934, and artesunate (ATS). (B) Four-week-old female mice received subcutaneous DHEA injections (60 mg/kg/day) along with intraperitoneal ATM injections (30 mg/kg/day) for 60 days. Subsequently, the mice were assessed for (C) serum testosterone ($n = 6$ to 12 biological replicates of mice), (D) estrous cycle analysis, and (E) hematoxylin and eosin (H&E) staining of representative ovaries showing cystic follicle or atretic follicle (asterisk), antral follicle (hash symbol), and corpora lutea or corpus albicans (arrow; scale bars, 200 μ m). (F) After the establishment of a DHEA-induced (60 mg/kg/day) PCOS-like model, mice were administered varying dosages of ATM (30 mg/kg/day and 60 mg/kg/day) via intraperitoneal injection and then evaluated for (G) serum testosterone ($n = 6$ per group), (H) estrous cycle analysis, (I) morphology of uterus, and (J) H&E staining of representative ovaries showing cystic follicle or atretic follicle (asterisk), antral follicle (hash symbol), and corpora lutea or corpus albicans (arrow; scale bars, 200 μ m). (K) After establishment of DHEA-induced (60 mg/kg/day) PCOS-like model, the mice received intragastric administration of ATM (100 mg/kg/day) and were then assessed for (L) serum testosterone ($n = 6$ to 8 per group), (M) estrous cycle analysis, (N) morphology of uterus, and (O) H&E staining of representative ovaries showing cystic follicle or atretic follicle (asterisk), antral follicle (hash symbol), and corpora lutea or corpus albicans (arrow; scale bars, 200 μ m). P, proestrus; E, estrus; M, metestrus; D, diestrus. Data are presented as mean \pm SD. Data in (C) were analyzed with Kruskal-Wallis test. Data in (G) and (L) were analyzed with Brown-Forsythe and Welch analysis of variance (ANOVA) tests with Tamhane's T2 multiple comparisons test. * $P < 0.05$, ** $P < 0.01$.



decrease serum testosterone in PCOS-like rats to levels similar to those of control rats (Fig. 2B) and to alleviate the disrupted estrous cycles (Fig. 2C). Ovarian histological analysis revealed that ATM reversed the oligo-ovulatory phenotype in DHEA-treated rats, as indicated by an elevation of postovulation corpora lutea and a decrease in cyst-like follicles (Fig. 2D). Similarly, oral administration of ATM also re-

pressed PCOS-like manifestations in the rat model (fig. S2, A to C).

The findings were further validated in another PCOS-like rat model established by insulin and hCG injections (Fig. 2E), both of which are robust inducers of androgen production. ATM treatment significantly ($P = 0.0026$) decreased serum testosterone in PCOS-like rats (Fig. 2F), totally normalized estrous cycles

(Fig. 2G), inhibited polycystic ovary morphology, and increased the presence of postovulation corpora lutea (Fig. 2H). Fertility tests showed that ATM dramatically enhanced embryo implantation (Fig. 2I) and significantly ($P = 0.0039$) elevated the litter size in PCOS-like rats (Fig. 2J). Collectively, the key features of PCOS, including elevated serum testosterone, irregular estrous cycle, polycystic ovarian

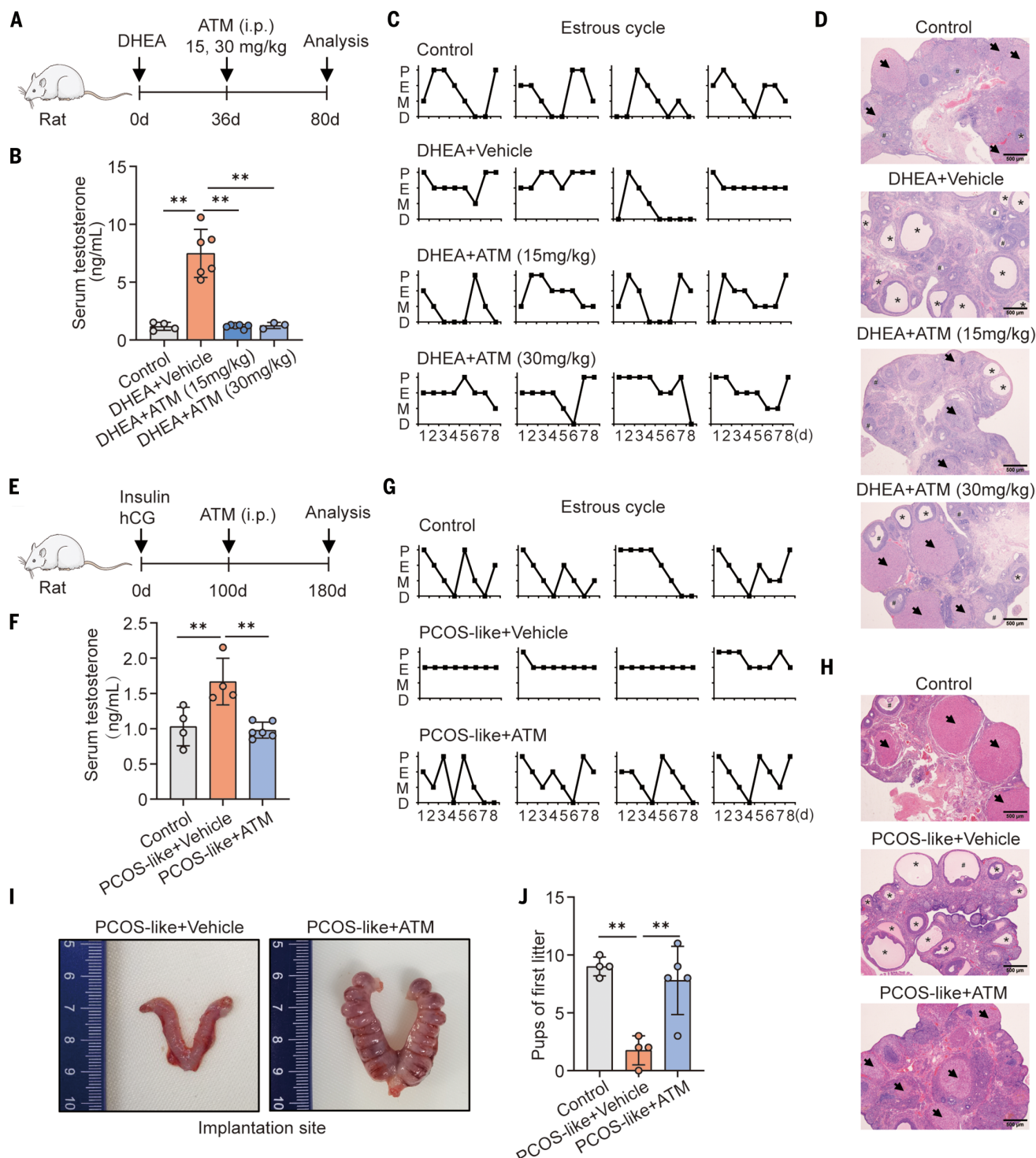


Fig. 2. ATM reverses the PCOS-like phenotype in a rat model. (A) Four-week-old female rats were subcutaneously injected with DHEA (60 mg/kg/day) to establish a PCOS-like model and then received intraperitoneal treatments of ATM (15 mg/kg/day and 30 mg/kg/day). Subsequently, the rats were assessed for (B) serum testosterone ($n = 3$ to 6 biological replicates), (C) estrous cycle analysis, and (D) H&E staining of representative ovaries showing cystic follicle or atretic follicle (asterisk), antral follicle (hash symbol), and corpora lutea or corpus albicans (arrow; scale bars, 500 μm). (E) Four-week-old female rats were subcutaneously injected with hCG and insulin to establish a PCOS-like model and then received intraperitoneal treatments of ATM (30 mg/kg/day). Thereafter, the rats underwent the following assessments:

(F) measurement of serum testosterone ($n = 4$ to 6 biological replicates), (G) estrous cycle analysis, and (H) H&E staining of representative ovaries showing cystic follicle or atretic follicle (asterisk), antral follicle (hash symbol), and corpora lutea or corpus albicans (arrow; scale bars, 500 μm). (I and J) The indicated female rats were paired with proven stud males for mating and evaluated for (I) uterine implantation and (J) the quantity of pups in the first litter ($n = 4$ to 5 biological replicates). P, proestrus; E, estrus; M, metestrus; D, diestrus. Data are presented as mean \pm SD. Data in (B) were analyzed with Brown-Forsythe and Welch ANOVA tests with Tamhane's T2 multiple comparisons. Data in (F) and (J) were analyzed with one-way ANOVA with Bonferroni's multiple comparisons test. ** $P < 0.01$.

morphology, and low fertility, were improved by ATM treatment in rodent models.

Artemisinins inhibit steroidogenesis and testosterone production in the ovary

The dramatic reduction in testosterone caused by ATM prompted us to explore the role of artemisinins in modulating androgen synthesis. The hypothalamus-pituitary-ovary axis plays a pivotal neuroendocrine role in androgen production (20). Therefore, we initially determined follicle-stimulating hormone (FSH) and LH, which are upstream hormones controlling the synthesis of steroid hormones, including progesterone, androgens, and estrogen (20). ATM displayed no impact on FSH and LH, whether administered intraperitoneally or orally in the PCOS-like models (fig. S3, A to F), implying that gonadotropin generation might remain unaltered by ATM. We therefore hypothesized that artemisinins regulated testosterone levels by targeting the ovary. To assess this, we measured steroid hormones in the supernatant of isolated ovarian theca-interstitial cells, which are a major source of excess testosterone biosynthesis in women with PCOS (Fig. 3A) (11). ATM significantly ($1 \mu\text{M}$ versus $0 \mu\text{M}$, $P = 0.0298$; $5 \mu\text{M}$ versus 0 , $P = 0.0011$; $10 \mu\text{M}$ versus 0 , $P = 0.0007$) inhibited testosterone production in theca-interstitial cells in a dose-dependent manner (Fig. 3B). Similarly, SM934, also an artemisinin analog (21), showed inhibitory effects on testosterone levels comparable to those induced by ATM (Fig. 3C). In addition to reducing testosterone, ATM and SM934 also obviously reduced pregnenolone, progesterone, and 17α -OHP, all of which are intermediates of ovarian steroidogenesis and the precursors of testosterone (Fig. 3, D to I). This observation was further validated with another artemisinin derivative, artesunate (ATS), which likewise dose-dependently suppressed pregnenolone, progesterone, and 17α -OHP (fig. S4, A to C). Moreover, this inhibitory effect was not due to cell toxicity because artemisinins did not impair the viability of theca-interstitial cells (fig. S5, A and B). These data strongly suggested that artemisinins inhibited the steroidogenic process and subsequent androgen synthesis in ovarian theca-interstitial cells.

Adipose tissue prominently expresses aldoketoreductase type 1C3 (AKR1C3), converting androstenedione (A4) to testosterone (22, 23). In conditions such as PCOS or obesity, elevated AKR1C3 in subcutaneous fat, possibly induced by increased insulin, endows adipose tissue as an important site for androgen synthesis (22, 23). However, ATM did not affect testosterone production in rat adipocytes both in the basal state and under insulin or A4 treatment (fig. S5C). Similarly, ATM showed no impact on testosterone production in human adipocytes (fig. S5D). Consistently, testosterone

concentration in rat adipose tissues remained unchanged by ATM treatment (fig. S5E).

Artemisinins limit testosterone production by reducing CYP11A1

To uncover the cellular pathways responsible for the decrease in androgen synthesis induced by artemisinins, we conducted mass spectrometry-based relative quantitative proteomics analysis on isolated theca-interstitial cells with or without ATM treatment. CYP11A1 was the most significantly ($P = 0.00000533$) down-regulated protein induced by ATM (Fig. 3J). CYP11A1 catalyzes the conversion from cholesterol to pregnenolone, which is the initial step of steroid hormone biosynthesis (12). The down-regulation of CYP11A1 by ATM coincided with the observation that artemisinins inhibited androgen synthesis from the first step, as evidenced by the decreased pregnenolone (Fig. 3D and G). To validate the proteomics data, we detected the expression of steroidogenic enzymes in theca-interstitial cells from mice and rats, with the results that artemisinins dose-dependently down-regulated CYP11A1 protein (Fig. 3K and fig. S6, A to C), whereas they did not affect HSD3B2 and CYP17A1 (Fig. 3K). The decline in CYP11A1 protein initiated at the 8th-hour post-ATM treatment (fig. S6D). Consistently, CYP11A1 proteins were dramatically reduced by ATM in the ovaries of PCOS-like mice (Fig. 3L). Furthermore, CYP11A1 was also down-regulated by artemisinins in human BeWo choriocarcinoma cells, which are human placenta-derived and can synthesize steroid hormones (fig. S6E). ATM treatment did not inhibit the steroidogenic acute regulatory (StAR) protein (fig. S6F), which is essential for translocating cholesterol from the outer to the inner mitochondrial membrane to facilitate steroid hormone formation (24).

Next, we proceeded to elucidate whether the decrease in CYP11A1 mediated the inhibitory effect of artemisinins on testosterone synthesis. First, we supplemented artemisinin-treated theca-interstitial cells with pregnenolone, which is the product of CYP11A1 catalytic reaction and reduced by artemisinins (Fig. 3A), with the results that pregnenolone replenishment dramatically reversed the decreased progesterone, 17α -OHP, and testosterone induced by artemisinins (Fig. 3M). We then manipulated the expression of CYP11A1 and found that overexpression of CYP11A1 fully rescued the decreased testosterone in artemisinin-treating cells (Fig. 3N). When CYP11A1 expression was disrupted, artemisinins were unable to further reduce the production of progesterone, 17α -OHP, and testosterone (Fig. 3O). These results together suggested that up-regulating and down-regulating CYP11A1 determined testosterone production and that artemisinins affected testosterone production through CYP11A1.

Artemisinins mediate the interaction between LONP1 and CYP11A1

We then aimed to explore the mechanism underlying the regulation of CYP11A1 by artemisinins. Although artemisinins act as endoperoxides and demonstrate antimalarial activity by generating reactive oxygen species (ROS) (25), it seemed that ROS alone was not involved in the down-regulation of CYP11A1, because the ROS inducer elesclomol had no detectable effect on CYP11A1 (fig. S7A). Consistently, ROS-scavenger N-Acetyl-L-cysteine (NAC) did not affect the ATM-induced down-regulation of CYP11A1 (fig. S7B). Additionally, despite the reduction in protein levels induced by artemisinins, the mRNA of *Cyp11a1* in isolated theca-interstitial cells (fig. S7, C and D) or DHEA-induced ovaries (fig. S7, E and F) remained unaffected by artemisinins, indicating posttranscriptional regulation by artemisinins. Subsequently, we examined the stability of CYP11A1 and found that the half-life of CYP11A1 protein was obviously shortened by ATM and SM934 (Fig. 4A and fig. S8A). Further study showed that the protease inhibitor MG132 rescued the down-regulation of CYP11A1 induced by ATM and SM934 (Fig. 4B and fig. S8B), which collectively indicated that artemisinins reduced CYP11A1 levels by repressing its protein stability.

To define the mediators responsible for artemisinin-induced instability of CYP11A1, we applied immunoprecipitation coupled with mass spectrometry (IP-MS) to identify the interacting partners of CYP11A1 under ATM or SM934 treatment (Fig. 4C). On the basis of the IP-MS data, we identified 8 proteins that interacted with CYP11A1 specifically under ATM treatment and 23 proteins that did so under SM934 treatment. Among these proteins, two candidates were found to be common in both groups, namely lon peptidase 1 (LONP1) and trafficking from ER to Golgi regulator (TFG) (Fig. 4C). LONP1 is an AAA+ mitochondrial protease and functions by utilizing ATP hydrolysis to degrade misfolded or oxidized proteins, which is crucial in protein quality control in mitochondria (26). TFG is a COPII vesicle-related protein that regulates ER to Golgi transport (27). To validate the IP-MS results, we conducted co-immunoprecipitation (co-IP) assay by precipitating CYP11A1-Flag and found that interaction between LONP1 and CYP11A1 was dramatically enhanced by ATM and SM934 induction, although precipitated CYP11A1 in the artemisinin-treated group was even lower than in control, primarily because of down-regulated CYP11A1 by artemisinin treatment (Fig. 4D). By contrast, TFG-CYP11A1 interaction could be slightly augmented by ATM but not SM934 (fig. S9A). Subsequent investigations revealed that LONP1 overexpression dramatically down-regulated CYP11A1 (fig. S9B), whereas TFG had no effect on it (fig. S9C). These data together suggested that LONP1 but not TFG might be

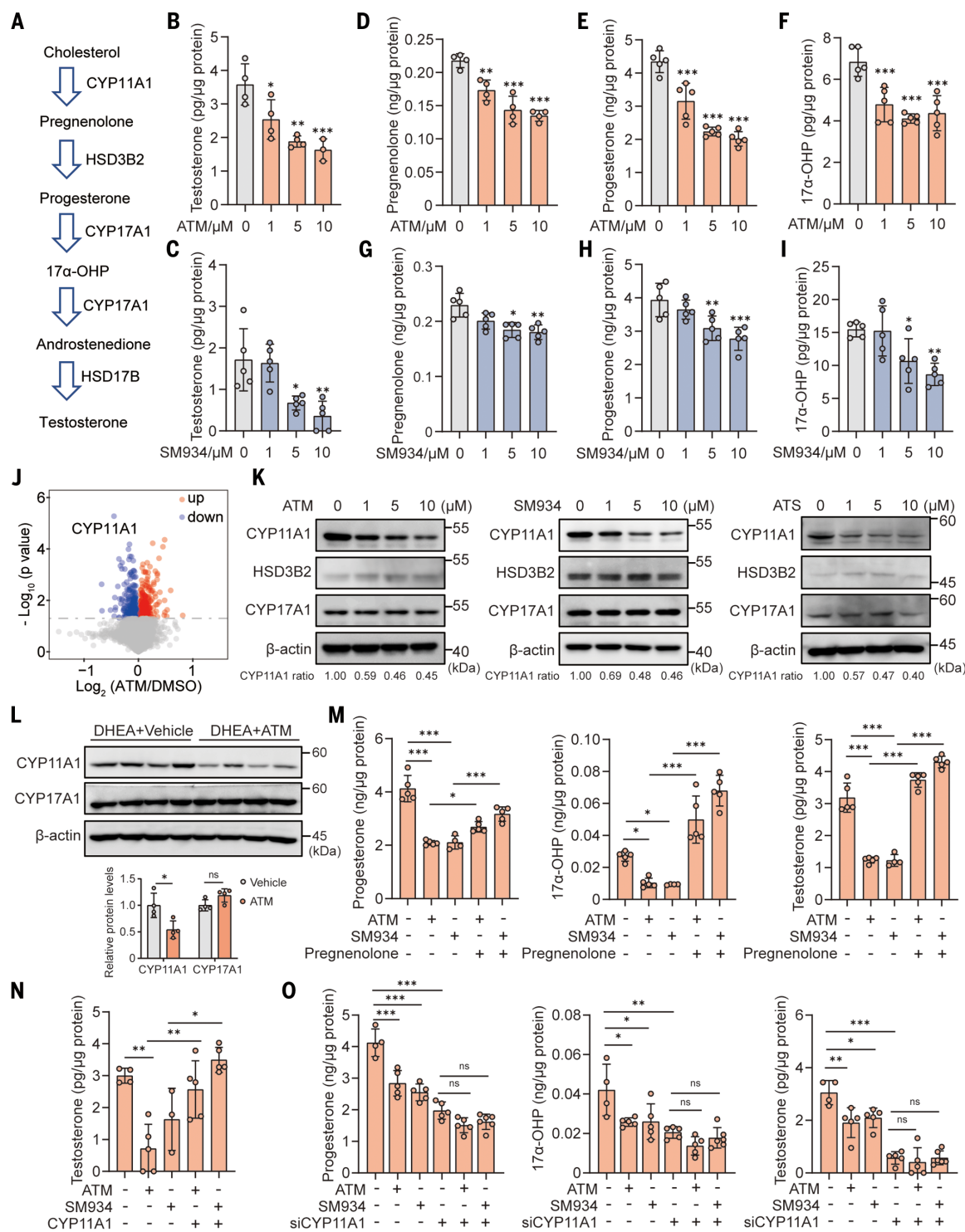


Fig. 3. Artemisinins inhibit ovarian steroidogenesis and testosterone production through down-regulation of CYP11A1. (A) Schematic diagram of ovarian testosterone production. (B to I) Mouse ovarian theca-interstitial cells were treated with various dosages of ATM or SM934 for 48 hours. Testosterone in the cell supernatant under ATM [(B), $n = 3$ to 4 biological replicates per group] and SM934 treatment [(C), $n = 5$ per group] were quantified and normalized to the total protein content. Pregnenolone [(D), $n = 4$ per group], progesterone [(E), $n = 5$ per group], and 17 α -OHP [(F), $n = 5$ per group] were measured in ATM-treated cells. Pregnenolone [(G), $n = 5$ per group], progesterone [(H), $n = 5$ per group], and 17 α -OHP [(I), $n = 5$ per group] were measured in SM934-treated cells. (J) Mouse ovarian theca-interstitial cells were treated with ATM (5 μ M) for 48 hours, followed by MS-based quantitative proteomics analysis ($n = 3$ biological replicates). Volcano plots illustrate the significant ($P < 0.05$) alterations in protein expression induced by ATM. (K) Isolated mouse ovarian theca-interstitial cells were treated with varying doses of ATM, SM934, or ATS for 48 hours. Representative Western blot analysis of CYP11A1, CYP17A1, and HSD3B2. CYP11A1 quantification, normalized to the loading control, was calculated on the basis of three repeated experiments. (L) Western blot analysis and relative quantification of CYP11A1 and CYP17A1 in the ovary from mice receiving intragastric administration of ATM.

group] were measured in SM934-treated cells. (J) Mouse ovarian theca-interstitial cells were treated with ATM (5 μ M) for 48 hours, followed by MS-based quantitative proteomics analysis ($n = 3$ biological replicates). Volcano plots illustrate the significant ($P < 0.05$) alterations in protein expression induced by ATM. (K) Isolated mouse ovarian theca-interstitial cells were treated with varying doses of ATM, SM934, or ATS for 48 hours. Representative Western blot analysis of CYP11A1, CYP17A1, and HSD3B2. CYP11A1 quantification, normalized to the loading control, was calculated on the basis of three repeated experiments. (L) Western blot analysis and relative quantification of CYP11A1 and CYP17A1 in the ovary from mice receiving intragastric administration of ATM.

(100 mg/kg/day) ($n = 4$ biological replicates). (M) Isolated ovarian theca-interstitial cells were treated with 5 μ M ATM or SM934 for 48 hours, either with or without 0.5 μ M pregnenolone. Progesterone, 17 α -OHP, and testosterone in the cell supernatant were measured and normalized to total protein ($n = 4$ to 5 biological replicates). (N) CYP11A1 was overexpressed in isolated ovarian theca-interstitial cells. Following a 48-hour incubation with 5 μ M ATM or SM934, the testosterone in the cell supernatant was detected and normalized to total protein content ($n = 3$ to 5 biological replicates). (O) CYP11A1 expression was

disrupted in ovarian theca-interstitial cells. Following a 48-hour incubation with 5 μ M ATM or SM934, progesterone, 17 α -OHP, and testosterone in cell supernatant were detected and normalized to total protein ($n = 4$ to 6 biological replicates). Data are presented as mean \pm SD. Bar graphs in (B) to (F), (H) and (I), and (M) to (O) were analyzed with one-way ANOVA with Bonferroni's multiple comparisons test. Data in (G) were analyzed with Kruskal-Wallis test with Dunn's multiple comparison test. Data in (L) were analyzed with two-tailed unpaired Student's *t*-test. * $P < 0.05$; ** $P < 0.01$; *** $P < 0.001$.

involved in regulating CYP11A1 protein levels. Endogenous co-IP further validated that binding affinity between LONP1 and CYP11A1 was augmented by ATM and SM934 (Fig. 4E and fig. S9, D and E). A pull-down assay with purified recombinant proteins of LONP1 and CYP11A1 confirmed a direct binding between these two proteins (fig. S9F). Taken together, these data strongly suggested that artemisinins enhanced CYP11A1-LONP1 association, acting like “molecular glues,” a class of small molecules that induce or stabilize interactions between proteins (28).

We next explored the functional regions of LONP1 and CYP11A1 that mediated their interaction. Protein-protein docking predicted that residues W56 to S66 or F252 to T259 in CYP11A1 might serve as the binding site for LONP1. We therefore generated mutant forms of CYP11A1 with deletion of either W56 to S66 (Δ W56-S66) or F252 to T259 (Δ F252-T259) and found that Δ W56-S66 retained the ability to interact with LONP1, whereas Δ F252-T259 lost the capacity to bind to LONP1 (Fig. 4F), suggesting that the region F252 to T259 in CYP11A1 was essential for CYP11A1-LONP1 interaction. To define the domain in LONP1 responsible for binding to CYP11A1, we expressed the N-domain, adenosine triphosphatase (ATPase) domain, and proteolytic domain of LONP1. Because LONP1 is a mitochondrial protein, we fused all the truncated domains with the mitochondrial targeting sequence (MTS) of LONP1 to ensure their import into the mitochondria (Fig. 4G). Unexpectedly, all the domains of LONP1 exhibited strong interactions with CYP11A1, without domain selectivity (Fig. 4H).

LONP1 promotes CYP11A1 degradation and inhibits testosterone synthesis

Having established that artemisinins augmented CYP11A1-LONP1 interaction, we then sought to investigate the role of LONP1 in artemisinin-induced CYP11A1 degradation. LONP1 overexpression reduced CYP11A1 levels, which were rescued by MG132 (Fig. 5A), which is a protease inhibitor also capable of inhibiting LONP1 (29). These results were in concert with the aforementioned data showing that MG132 could restore the decreased CYP11A1 caused by artemisinins (Fig. 4B). Additionally, the reduced CYP11A1 expression caused by ATM was

reversed by the inhibitor of LONP1, methyl ester derivative of 2-cyano-3,12-dioxo-oleana-1,9(11)-dien-28-oic acid (CDDO-Me) (30) (Fig. 5B). Knockdown of LONP1 in theca-interstitial cells with two sets of small interfering RNAs (siRNAs) completely reversed the decreased CYP11A1 induced by ATM (Fig. 5C). In LONP1-deficient cells, ATM had little effect on the down-regulation of CYP11A1 (Fig. 5C). By contrast, CYP17A1 remained unaffected by both ATM and LONP1 (Fig. 5C). Subsequently, we generated catalytically inactive LONP1 (LONP1-S844A) with an S844A (S844 \rightarrow A) substitution that disrupts the catalytic dyad responsible for protein degradation (31, 32). LONP1-S844A failed to diminish CYP11A1 expression (Fig. 5D) or shorten the half-life of CYP11A1 protein (Fig. 5E) like the WT LONP1 did, indicating that LONP1 decreased CYP11A1 through its protease activity. To confirm whether LONP1 directly mediated the down-regulation of CYP11A1, we conducted *in vitro* protease assay using purified CYP11A1 and LONP1 proteins. The presence of ATP was necessary for LONP1's function. Our results showed that ATM promoted the LONP1-catalyzed degradation of CYP11A1 (Fig. 5F), whereas in the absence of LONP1 or ATP, ATM had no effect on CYP11A1 (Fig. 5F). The *in vitro* protease assay further confirmed that both ATM and SM934 accelerated LONP1-catalyzed degradation of CYP11A1 (Fig. 5G). Besides, the mutant form of CYP11A1 (Δ F252-T259), which failed to bind with LONP1, exhibited resistance to the down-regulation induced by artemisinins (fig. S9, G and H). These observations collectively supported the indispensable role of LONP1 in mediating the reduction of CYP11A1 induced by artemisinins. Additionally, we found that both LONP1 and CYP11A1 were highly expressed in ovaries (fig. S9I), and they are known to be localized in mitochondria (12, 33). The similar tissue distribution and subcellular localization suggested the possibility that LONP1 could target CYP11A1 in response to artemisinin treatment.

In addition to LONP1, the ClpXP complex, another important protease machinery in mitochondrial matrix responsible for protein quality control (34), was also examined for its involvement in regulating CYP11A1. ClpXP consists of two distinct components, an AAA+ ATPase called ClpX and a peptidase known as ClpP (34). Overexpression of both ClpP and ClpX

had no impact on CYP11A1 protein (fig. S10A). Additionally, no binding was observed between CYP11A1 and either ClpP or ClpX, and artemisinins did not promote their interaction (fig. S10B). These findings rule out the possibility of ClpXP in mediating CYP11A1 degradation.

Next, we assessed the impact of LONP1 on ovarian androgen synthesis. Adenovirus-mediated overexpression of LONP1 in theca-interstitial cells or BeWo cells down-regulated CYP11A1 protein (Fig. 5H and fig. S11A). As a consequence of decreased CYP11A1, the supernatant levels of pregnenolone, progesterone, 17 α -OHP, and testosterone from theca-interstitial cells were considerably reduced by LONP1 overexpression (Fig. 5, I to L). Consistent with this, overexpression of LONP1 in BeWo cells also yielded a reduction in steroidogenesis (fig. S11, B and C). We also overexpressed LONP1 in ovaries of mice by intraperitoneal injection of adeno-associated virus (AAV)-LONP1, with the results that LONP1 reduced CYP11A1 (Fig. 5M) and concomitantly inhibited the serum testosterone (Fig. 5N). These data together suggested that overexpression of LONP1 replicated the androgen-lowering effect of artemisinins.

Publicly available data from the Gene Expression Omnibus (GEO, accession no. GSE1615) indicated that LONP1 expression levels in theca cells from PCOS patients were significantly ($P = 0.0104$) lower as compared with levels found in normal theca cells (Fig. 5O) (35), which was in line with the inhibitory effect of LONP1 on CYP11A1 and androgen synthesis. We further examined the CYP11A1-LONP1 association in response to androgen inducers, such as hCG (36). In contrast to the promoting effect of artemisinins on CYP11A1-LONP1 interaction, hCG markedly disrupted their interaction (fig. S12A). Consequently, hCG treatment promoted CYP11A1 levels and reversed the decreased CYP11A1 caused by LONP1 overexpression (fig. S12B). Consistent with this result, CYP11A1 was elevated in the ovaries of the PCOS-like mouse model established by hCG and insulin treatment (fig. S12C). Furthermore, dihydrotestosterone (DHT), one type of androgen, also recovered the decreased CYP11A1 caused by LONP1 (fig. S12D). These data together indicated that androgenic inducers blocked the association between LONP1 and CYP11A1, promoted CYP11A1 expression, and thus could aggravate androgen excess.

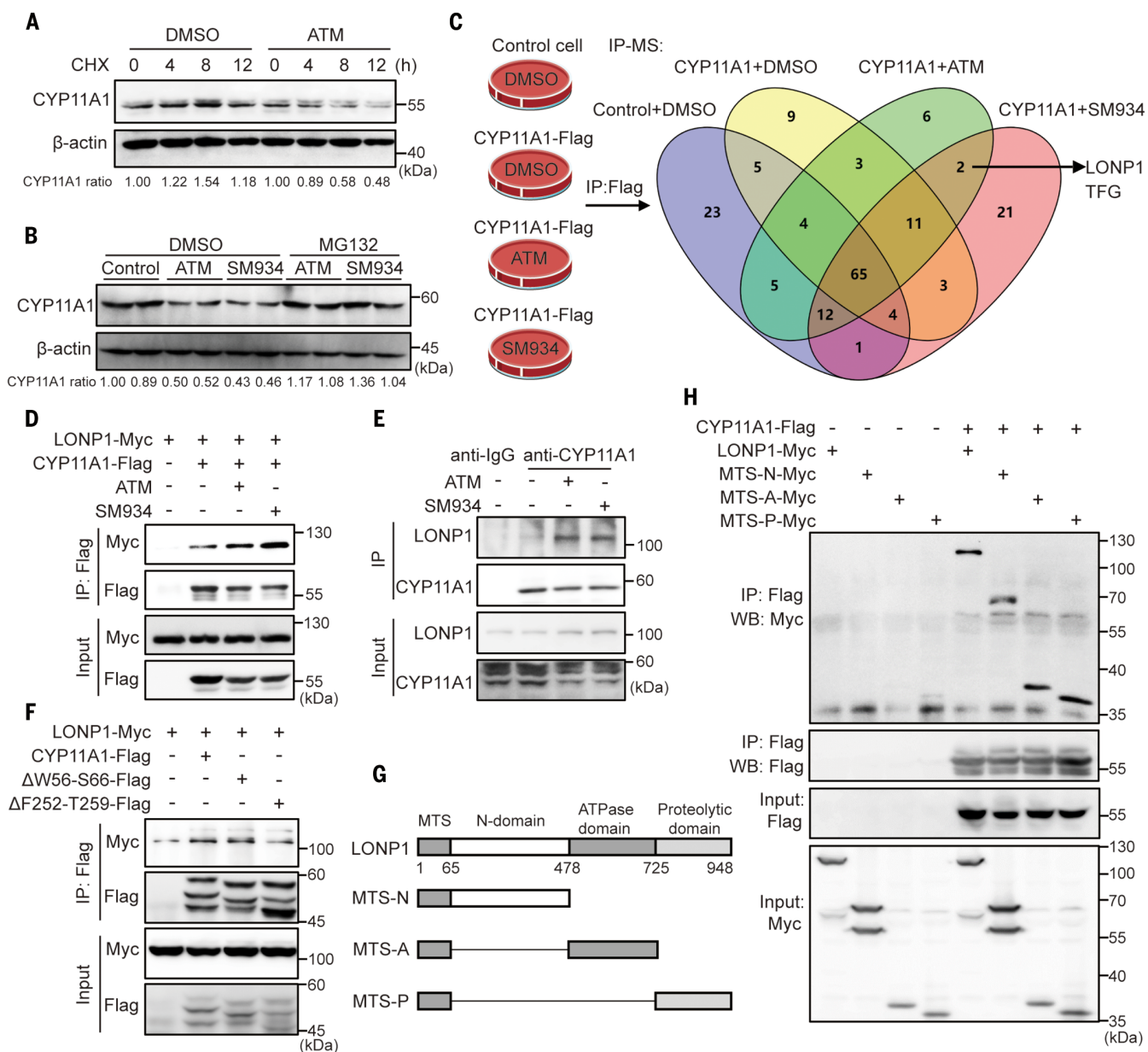


Fig. 4. Artemisinins enhance the interaction between LONP1 and CYP11A1.

(A) Isolated ovarian theca-interstitial cells pretreated with 5 μM ATM were incubated with cycloheximide (CHX) for indicated time, followed by analysis of the half-life of CYP11A1 protein. (B) Isolated ovarian theca-interstitial cells were treated with 5 μM ATM or SM934 for 12 hours, in either the presence or absence of MG132, followed by detection of CYP11A1. (C) CYP11A1 was stably overexpressed in human embryonic kidney 293T (HEK293T) cells. IP-MS was conducted to identify the artemisinin-responsive interacting proteins of CYP11A1. (D) HEK293T cells expressing specified protein were treated with 5 μM ATM or SM934 for 24 hours. IP was then conducted using Flag tag, followed by Western blot with a Myc antibody to detect the interacting LONP1. (E) In rat ovarian theca-interstitial cells treated with 5 μM ATM

or SM934 for 24 hours, endogenous IP was conducted with an anti-CYP11A1 antibody, followed by Western blot with a LONP1 antibody to detect the LONP1-CYP11A1 interaction. (F) LONP1 was coexpressed with wild-type (WT) or mutant CYP11A1 in HEK293T cells. IP was then conducted using Flag tag, followed by detection of the interacted LONP1 by Western blot with Myc antibody. Single-letter abbreviations for the amino acid residues are as follows: A, Ala; D, Asp; F, Phe; G, Gly; K, Lys; P, Pro; S, Ser; T, Thr; and W, Trp. (G) Different domains (N, N-domain; A, ATPase domain; P, proteolytic domain) were expressed in HEK293T cells that stably overexpressed CYP11A1. (H) IP was conducted with Flag tag, followed by detection of the interacting LONP1 domains with a Myc antibody. The experiments in (A), (B), and (D) to (H) were repeated at least two to three times.

LONP1 is the direct target of artemisinins

We then sought to ascertain whether artemisinins directly targeted LONP1 or CYP11A1. To this end, biotin was conjugated to artesunate (bio-ATS) for the pull-down assay (Fig. 6A). We confirmed that bio-ATS effectively reduced

CYP11A1 (fig. S13A), indicating that the biotin attachment did not affect the function of ATS. Subsequently, we conducted a bio-ATS capture assay and found that bio-ATS exhibited binding affinity toward the LONP1 protein instead of CYP11A1 (Fig. 6B and fig. S13B). Pre-

incubation with free ATS, ATM, or SM934 occupied LONP1 and disrupted the interaction between bio-ATS and LONP1 (Fig. 6B). Furthermore, the thermal stability assay provided additional evidence for the interaction between artemisinins and LONP1 (Fig. 6C), supported

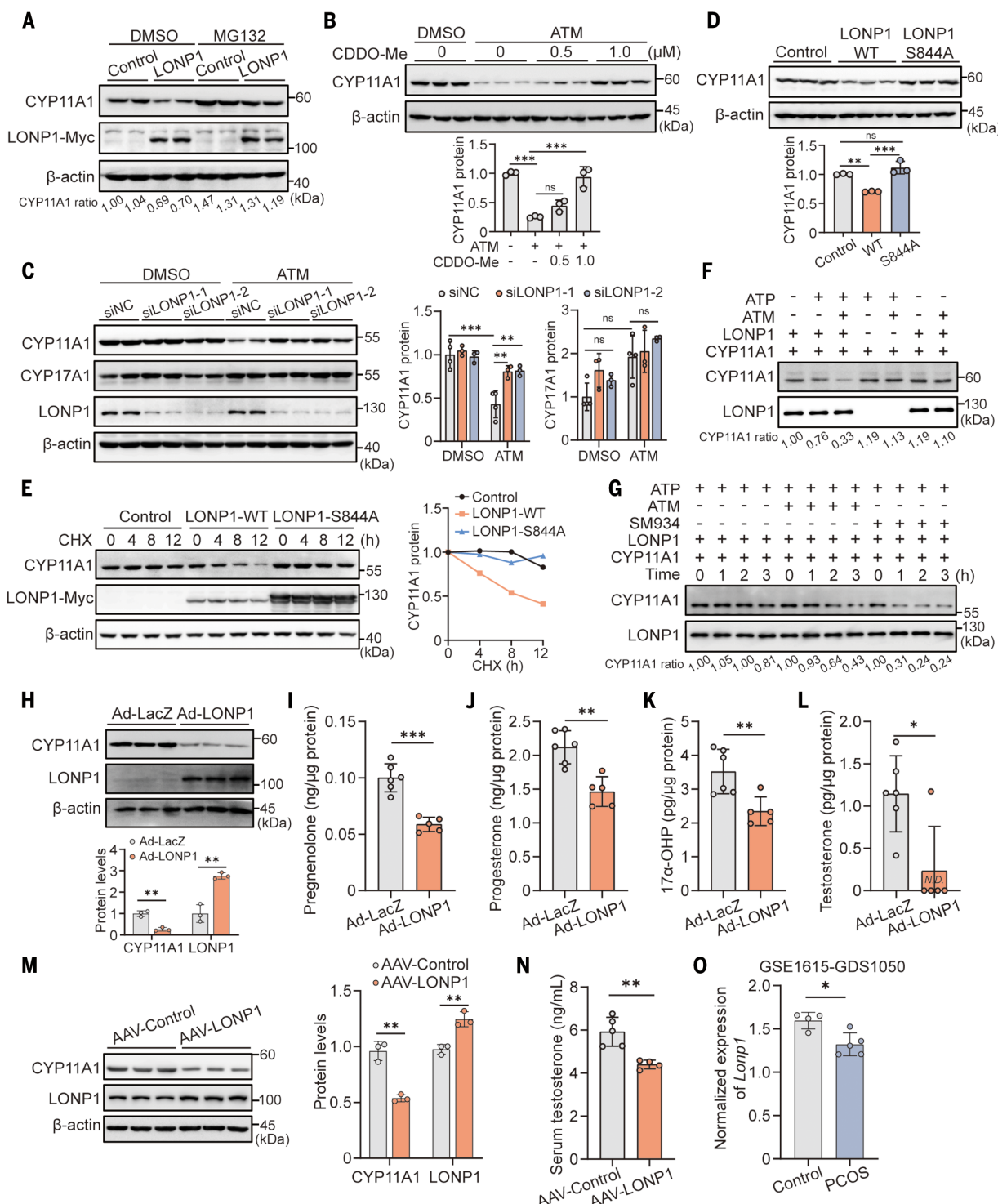


Fig. 5. LONP1 promotes the degradation of CYP11A1, leading to a reduction in androgen synthesis. (A) HEK293T cells stably expressing CYP11A1-Flag were subjected to LONP1-Myc overexpression and treated with MG132 for 8 hours, followed by detection and relative quantification of CYP11A1 by a Flag antibody and LONP1 by a Myc antibody. (B) HEK293T cells stably expressing CYP11A1-Flag were co-treated with 5 μM ATM and a specified dosage of CDDO-Me for 11 hours, then CYP11A1 was detected by a Flag antibody, and the blots were quantified ($n = 3$ biological replicates). (C) Isolated ovarian theca-interstitial cells were transfected with siNC or siLONP1 and treated with 5 μM ATM for 48 hours. CYP11A1 and CYP17A1 were detected and quantified from dependent

experiments ($n = 3$ to 4 biological replicates). (D) CYP11A1 levels were detected and quantified ($n = 3$ biological replicates) by a Flag antibody in HEK293T cells overexpressing WT-LONP1 and LONP1 (S844A). (E) The half-life of CYP11A1 was measured and quantified in HEK293T cells overexpressing WT-LONP1 or LONP1 (S844A) with a Flag antibody. (F and G) Analysis of protease reactions for 3 hours (F) and indicated time course (G) using purified LONP1 (400 ng) and CYP11A1 (400 ng) in vitro under 5 μM artemisinin treatment. (H) Western blot analysis of CYP11A1 and its quantification in ovarian theca-interstitial cells following LONP1 overexpression through adenovirus ($n = 3$ biological replicates). (I to L) Pregnenolone (I), progesterone (J), 17α-OHP (K), and testosterone (L) in experiments ($n = 3$ to 4 biological replicates). (M) Western blot analysis of CYP11A1 and LONP1 in AAV-control and AAV-LONP1 mice. (N) Serum testosterone levels in AAV-control and AAV-LONP1 mice. (O) Normalized expression of GSE1615-GDS1050 in Control and PCOS groups.

the cell supernatant of ovarian theca-interstitial cells were measured and normalized to total protein content ($n = 5$ to 6 biological replicates). (M and N) LONP1 was overexpressed in the ovaries by intraperitoneal injection of AAV-LONP1 in mice. (M) CYP11A1 expression and its quantification in the ovaries ($n = 3$ biological replicates). (N) Serum testosterone was measured in LONP1-overexpressed and control mice ($n = 4$ to 5 biological replicates). (O) Publicly available data revealed LONP1 expression in theca cells derived from PCOS

patients and healthy controls (GEO accession no. GSE1615, $n = 4$ to 5 biological replicates). Data are presented as mean \pm SD. Bar graphs in (B), CYP11A1 in (C) and data in (D) were analyzed by one-way ANOVA with Bonferroni's multiple comparisons test. Data for CYP17A1 in (C) were analyzed by using Kruskal-Wallis test with Dunn's multiple comparisons test. Data in (H) to (K) and (M) to (O) were analyzed with two-tailed unpaired Student's *t*-test. Bar graph in (L) was analyzed with Mann-Whitney test. * $P < 0.05$, ** $P < 0.01$, *** $P < 0.001$.

by the concept that compound binding can induce changes in protein conformation, thereby affecting thermal stability. By contrast, ATM had no impact on the thermal stability of CYP11A1 (fig. S13C). These data collectively suggested that LONP1, rather than CYP11A1, is the direct target of artemisinins.

To study the binding modes of artemisinin to its target, a protein structure-based docking calculation was carried out with a 2.51-Å resolution structure of LONP1 (PDB entry: 6WZV) (37) by using Glide v8.1. Artemisinin derivative was successfully docked in silico against the known bortezomib binding pocket within the proteolytic domain of LONP1 (Fig. 6D). Bortezomib is a known inhibitor of LONP1 (37). We observed that bortezomib augmented CYP11A1 levels and reversed the decreased CYP11A1 induced by LONP1 (fig. S13D). This finding led us to speculate that if the docking simulation was accurate, bortezomib might compete with artemisinin for binding to LONP1. We therefore conducted a bio-ATS capture assay and discovered that preincubation of bortezomib blocked the interaction between bio-ATS and LONP1 (fig. S13E). In concert with the competition between bortezomib and artemisinin for binding to LONP1, bortezomib completely rescued the decreased CYP11A1 caused by artemisinins (fig. S13F). Considering that the predicted binding pocket of artemisinin was located within the proteolytic domain of LONP1, we produced and purified this domain and measured the binding affinity of artemisinins to it. Surface plasmon resonance (SPR) revealed that ATM bound with the proteolytic domain with a dissociation constant (K_D) of 3.11 ± 0.358 μM (Fig. 6E), SM934 exhibited a binding affinity with a K_D of 8.69 ± 0.749 μM (Fig. 6F), and ATS displayed a strong binding affinity with a K_D of 0.261 ± 0.029 μM (Fig. 6G). The interaction between proteolytic domain of LONP1 and CYP11A1 was augmented by artemisinin analog SM934 (Fig. 6H). We then generated a mutant form of LONP1 with a deletion of residues G847 to D852 (ΔGATPKD). These residues were found to be involved in the formation of LONP1-artemisinin binding, according to our docking data. The mutant ΔGATPKD LONP1 retained its capacity to interact with CYP11A1, similarly to WT LONP1, but it conferred resistance to artemisinins, as indicated by the observation that artemisinins failed to enhance the interaction between ΔGATPKD LONP1 and CYP11A1 (Fig. 6I). To functionally evaluate the

contribution of the GATPKD motif of LONP1 to artemisinin-induced CYP11A1 degradation, we generated LONP1 knockout cells and reconstituted them with either WT LONP1 or the mutant ΔGATPKD LONP1. Loss of LONP1 up-regulated CYP11A1 compared with the results for control cells. Reconstitution with either WT or mutant LONP1 successfully reversed the increased CYP11A1, indicating that mutant LONP1 still preserved its protease activity to degrade CYP11A1 (Fig. 6J). When these cells were treated with artemisinins, CYP11A1 was down-regulated in the control cells but remained unchanged in the LONP1 knockout cells. Reintroduction of WT LONP1 restored the inhibitory effect of artemisinins on CYP11A1, whereas reintroduction of mutant LONP1 failed to reverse the artemisinin-induced down-regulation of CYP11A1 (Fig. 6J), which could result primarily from the mutant LONP1's inability to bind to artemisinins. It was worth noting that the GATPKD residues in LONP1 were highly conserved across different species (fig. S13G), supporting the observed similar effect of artemisinins in lowering androgen levels in both rodent and human cells. Collectively, these data supported the idea that the inhibitory effect of artemisinins on CYP11A1 level was largely dependent on its binding to the proteolytic domain of LONP1.

Therapeutic effect of dihydroartemisinin in patients with PCOS

Lastly, we performed a pilot clinical study to validate the efficacy of artemisinins in treating patients with PCOS. Nineteen individuals with PCOS [female, age: 27.79 ± 3.74 years; weight: 62.1 ± 8.9 kg; body mass index (BMI): 23.23 ± 2.30 kg/m²] who met all three Rotterdam PCOS diagnostic criteria were recruited and treated with oral dihydroartemisinin (40 mg, thrice daily) for 12 weeks. All the participants exhibited hyperandrogenemia, oligomenorrhea, or amenorrhea, and polycystic ovary appearance before treatment. Dihydroartemisinin was well tolerated and no side effects were observed in any of the participants. Treatment with dihydroartemisinin significantly ($P < 0.0001$) reduced serum testosterone among individuals with PCOS (Fig. 7A). Anti-Müllerian hormone (AMH) is mainly produced by granulosa cells of the preantral and small antral follicles in the ovary. Serum AMH levels strongly correlate with the number of growing follicles and are therefore typically elevated in PCOS patients (3). Dihydroartemisinin treatment sig-

nificantly ($P < 0.0001$) decreased the serum AMH (Fig. 7B). Consistent with this result, a substantial reduction of antral follicle count after dihydroartemisinin treatment was observed on ultrasonography (Fig. 7C). Additionally, regular menstrual cycles were restored in 63.16% (12/19) of all patients with PCOS (Fig. 7D and fig. S14). Together, dihydroartemisinin effectively ameliorated the hyperandrogenemia, improved polycystic ovarian morphology, and contributed to the normalization of menstruation in PCOS patients.

Discussion

Artemisinin has shown great promise in various applications with minimum adverse effects, such as treating malaria, cold, diarrhea, lupus erythematosus, and cancer (18). Increasing evidence supports heme or its biosynthesis metabolism as the primary mechanism for the antimalaria function of artemisinins (38, 39). The endoperoxide moiety in artemisinins reacts with the iron in heme to produce ROS, which elicits cytotoxicity effects on parasites or tumor cells. Several targets of artemisinins have been proposed, including PfPI3K and PfATP6 in malaria parasites (40, 41) and gephyrin in mammalian cells (42). Nevertheless, there have been no previous clues indicative of the possible effect of artemisinins on PCOS intervention. Emerging evidence suggests that dysregulated metabolic pathways are involved in PCOS development, including impaired thermogenic adipose tissue (43), the microbiota-gut-ovary axis (44), and systemic insulin resistance (45). Our previous findings showed that artemisinins promoted metabolic homeostasis and protected against obesity (19), which prompted us to investigate whether artemisinins could regulate PCOS development. In this study, we observed that artemisinins exhibited benefits to the reproductive endocrine in the PCOS-like rodent models and patients, with efficacy against hyperandrogenism, irregular estrous cycles, and polycystic ovaries. However, in the preventive experiments, we did not observe an obvious metabolic effect of artemisinins in PCOS-like mouse model, indicating that the effect of artemisinins in alleviating PCOS might not rely on the improvement of systemic metabolic state.

The effect of artemisinins on steroidogenesis may be linked to their antimalaria function. Recently, it was reported that infection-responsive malaria-associated pregnenolone

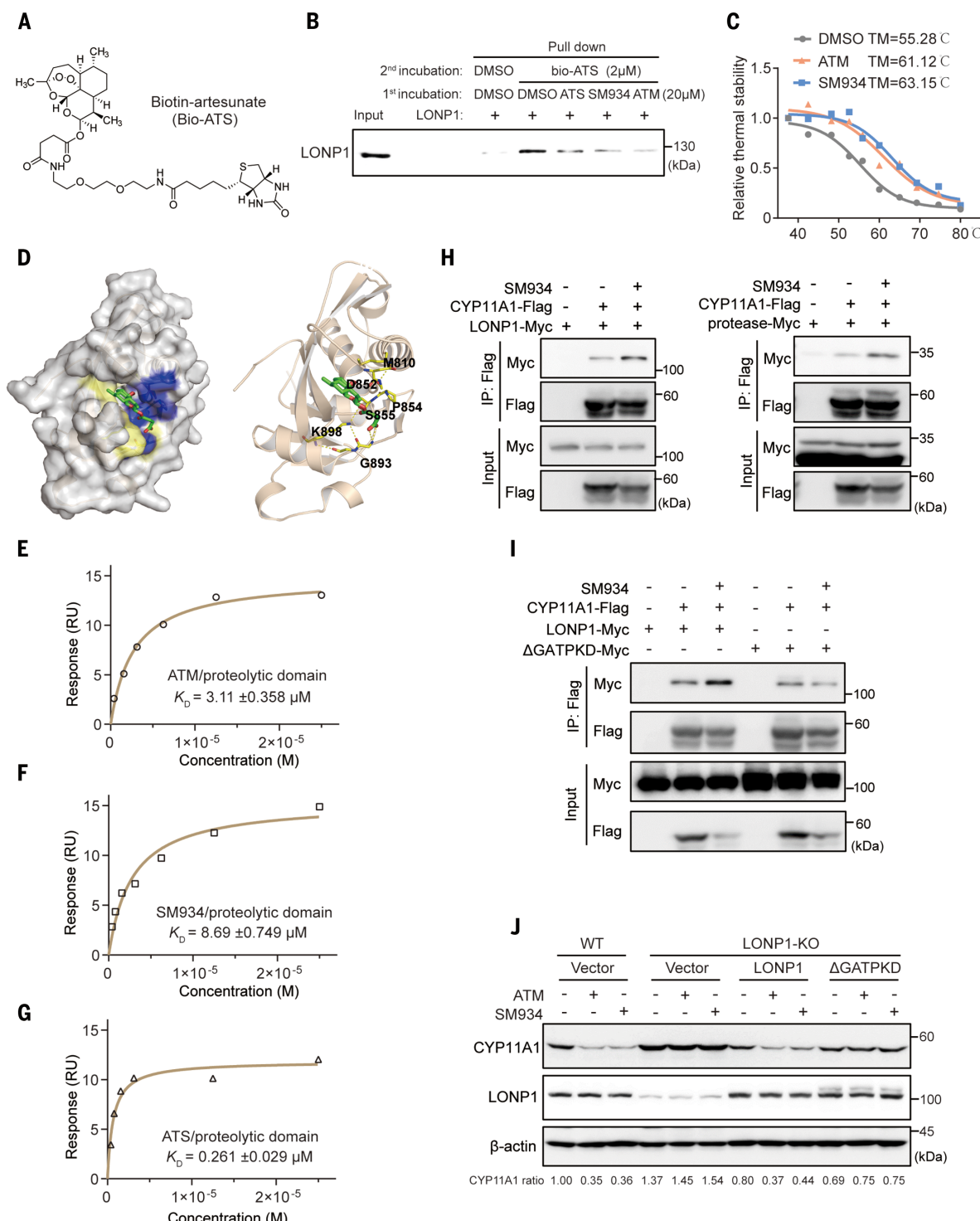


Fig. 6. LONP1 is the direct target of artemisinins. **(A)** Chemical structure of biotin-labeled artesunate (bio-ATS). **(B)** Purified LONP1 was preincubated with dimethyl sulfoxide (DMSO), 20 μ M free ATS, ATM, or SM934, followed by incubation with 2 μ M bio-ATS. Bio-ATS was then captured to detect interaction between LONP1 and artemisinins. **(C)** Thermal stability of LONP1 was evaluated following pretreatment with 5 μ M artemisinins for 30 min. **(D)** Docking model of the LONP1 and ATS. **(E to G)** SPR assay showing the interaction between purified LONP1 protease domain and ATM (E), SM934 (F), or ATS (G) respectively. The K_D value was calculated from three dependent experiments. **(H)** Full-length LONP1 or its proteolytic domain was transfected into HEK293T cells stably expressing

CYP11A1-Flag. After treatment with SM934 (5 μ M) for 24 hours, co-IP was conducted with Flag tag, followed by detection of the interacting LONP1 by Western blot with a Myc antibody. (I) WT LONP1 or mutant LONP1 (with GATPKD deletion) was expressed in HEK293T cells stably expressing CYP11A1-Flag. After treatment with SM934 (5 μ M) for 24 hours, co-IP was conducted with Flag tag, followed by detection of the interacting LONP1 by Western blot with a Myc antibody. (J) LONP1 knockout cells were reconstituted with WT LONP1 or mutant LONP1 (GATPKD deletion). The designated cells were treated with artemisinins (5 μ M) for 24 hours and subjected to detection and relative quantification of CYP11A1 expression. The experiments in (B) and (E) to (J) were repeated at least two to three times.

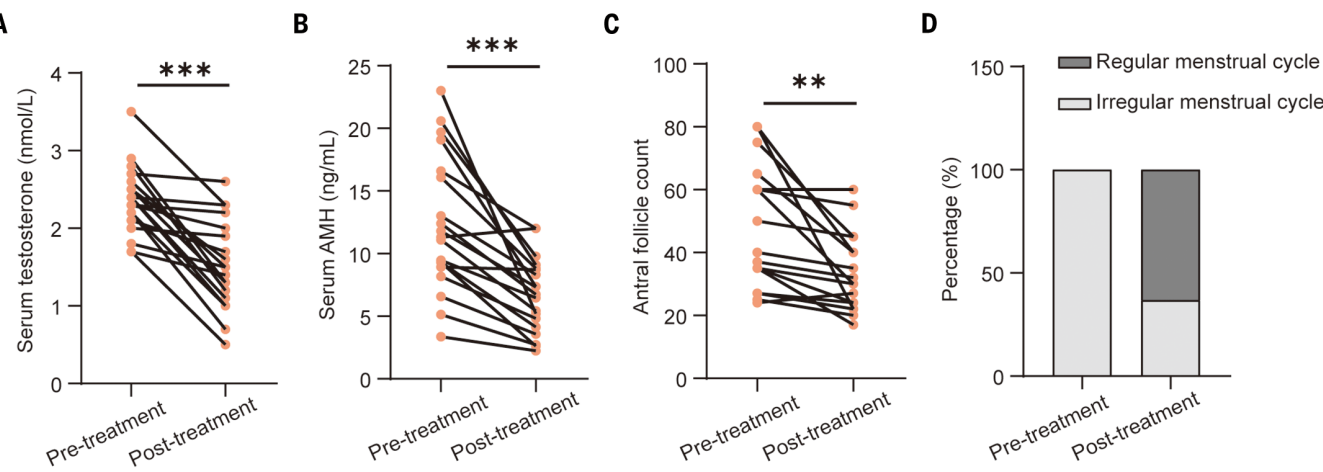


Fig. 7. Therapeutic effect of dihydroartemisinin in patients with PCOS. (A to D) Patients ($n = 19$) meeting all three PCOS diagnostic criteria were treated with oral dihydroartemisinin at a dosage of 40 mg three times daily for a duration of 12 weeks. Serum testosterone (A), AMH (B), antral follicle counts (C), and menstrual cycles (D) were assessed before and after dihydroartemisinin treatment. Bar graphs in (A) to (C) were analyzed by paired t-test. $^{**}P < 0.01$, $^{***}P < 0.001$.

steroid elevation exhibited an immunosuppressive effect on T cells and exacerbated malaria (46). Considering our observation that artemisinins inhibit pregnenolone production, it would be worthwhile to test whether artemisinins can restore pregnenolone levels in malaria patients, thereby repressing the infection. The antimalaria function of artemisinins is facing substantial challenges. The resistance of malaria parasite to artemisinins has been documented for approximately 20 years (47, 48). The global concern about artemisinin resistance in malaria control has persisted over this extended period. Although not the initiating factor for artemisinin resistance, the broader application of artemisinins for nonmalarial conditions, such as potential future use in PCOS treatment, may possibly accelerate the development of resistance. Nevertheless, because the mechanisms of artemisinins for treating PCOS and malaria might be different, it may become possible to enhance the efficacy of artemisinins for PCOS treatment while minimizing their impact on malaria by developing artemisinin derivatives. Besides, emerging therapies such as malaria vaccines are gradually reshaping the landscape of malaria treatment, which might reduce reliance on artemisinins in the future.

Establishing an animal model that accurately mirrors PCOS in women is imperative. Several rodent models for PCOS have been reported, encompassing androgen-induced models (utilizing testosterone, DHT, and DHEA), estrogen-induced models, aromatase inhibitor-induced models, transgenic rodent models, and diet-induced models (49). Although the androgenic model has been considered the most reliable, none of these models fully replicates the complex conditions of PCOS in women (49). In this study, we used a peripubertal DHEA model, displaying elevated serum tes-

tosterone levels, irregular estrous cycles, and polycystic ovarian morphology. However, this model also exhibited other endocrinopathies including hyperprolactinemia, such that it did not fully mirror PCOS features in women—a limitation in the current study. Nonetheless, we also used an hCG- and insulin-induced model and integrated findings from a human pilot study to comprehensively assess the impact of artemisinins on PCOS development.

LONP1 is a highly conserved multifunctional enzyme responsible for mitochondrial quality control through preferentially degrading damaged, oxidized, or misfolded proteins, as well as acting as a chaperone for protein folding in mitochondria (34, 50–53). Here, we uncovered a function of LONP1 in controlling androgen synthesis by targeting CYP11A1 in response to artemisinins. CYP11A1 was involved in the inhibitory effect of artemisinins on steroidogenesis, whereas CYP17A1, HSD3B2, and StAR might not be. LONP1 and CYP11A1 shared similar tissue distribution patterns, being abundantly expressed in theca-interstitial cells of the ovary and localized within the mitochondria (54). However, under normal conditions, CYP11A1 remained relatively stable because of its minimal affinity for LONP1. By contrast, the presence of artemisinins enhanced LONP1-CYP11A1 interaction, leading to the degradation of CYP11A1 by LONP1. A previous study reported that artemisinins can locate into mitochondria (55), making it possible to mediate the LONP1-CYP11A1 interaction. The androgen-lowering effect indicates LONP1 as a promising target for hyperandrogenism intervention. LONP1 expression was decreased in the theca cells of PCOS as compared with levels in control, which could be a cause of the increased levels of CYP11A1 and androgens observed in PCOS. However, the inducer for the down-regulation of LONP1 in

PCOS remains unclear. LONP1 has been reported to decrease with age, oxidative stress, and disuse muscle atrophy (56, 57). Additionally, its activity is largely attenuated during mitochondrial dysfunction (58). Thus, we speculate whether PCOS-related oxidative stress or mitochondrial dysfunctional signal could potentially lead to the down-regulation of LONP1 expression or its activity. Additionally, a recent report documented the involvement of LONP1 in oocyte development and survival. Conditional disruption of LONP1 in mouse oocytes impairs follicular development and causes progressive oocyte death and infertility (59). Taken together with our current study, these findings highlight the profound role of LONP1 in both ovarian steroidogenesis and follicular development, indicating its potential application in the treatment of infertility.

Our findings indicate that artemisinins may serve as molecular-glue degraders that direct LONP1 to degrade CYP11A1. Classic molecular-glue degraders are drug-like compounds that induce or stabilize interactions between an E3 ubiquitin ligase and a target, resulting in the ubiquitination and subsequent degradation of the recruited protein (28, 60). This emerging strategy enables the depletion of therapeutic targets that were previously inaccessible by conventional pharmacological methods. Here, we demonstrated that, in addition to ubiquitin ligase, molecular glues can also directly hijack proteases such as LONP1 to facilitate target protein degradation by forming LONP1-substrate interactions. This degradation program may be responsive because it bypasses the ubiquitylation process. As LONP1 is located in mitochondria, we proposed a promising strategy for controlling protein degradation in the mitochondria based on molecular glues. Subsequent studies could focus on the design and development of new compounds based on

artemisinins that specifically enhance the interaction between LONP1 and CYP11A1. The objective would be to minimize any potential off-target effects of artemisinins on other targets of LONP1. Furthermore, we discovered a putative artemisinin binding pocket in the proteolytic domain of LONP1 and defined residues GATPKD within this pocket that are key for LONP1's response to artemisinins. Indeed, interaction between CYP11A1 and the proteolytic domain of LONP1 was augmented by artemisinins. However, the exact mechanism by which artemisinins reinforce the LONP1-CYP11A1 interaction remains unknown. We speculate that binding with artemisinins may induce conformational changes in LONP1 or modify LONP1 protein surface, allowing for enhanced interaction with CYP11A1. To test this hypothesis, a more detailed binding model of artemisinin-LONP1-CYP11A1 trimer will be needed.

Overall, we propose a model in which artemisinin derivatives protect against PCOS development by inhibiting ovarian androgen production. Artemisinins directly target LONP1 and induce LONP1-CYP11A1 interaction, thereby promoting CYP11A1 degradation and subsequently inhibiting ovarian androgen synthesis. Consequently, artemisinins show efficacy in ameliorating PCOS symptoms in both rodents and human patients. Conversely, the pro-androgen inducer hCG inhibits the LONP1-CYP11A1 association; additionally, LONP1 is down-regulated in PCOS, leading to up-regulation of CYP11A1, which in turn promotes androgen production and exacerbates PCOS. Our findings not only demonstrate the therapeutic effect of artemisinins on PCOS patients but also highlight their potential as molecular-glue degraders. This discovery opens up avenues for controlling ovarian androgen synthesis by targeting the LONP1-CYP11A1 interaction.

Materials and methods

Animal model

All the C57BL/6J mice (Cat no. N000013) were purchased from Gempharmatech Co., Ltd. (Nanjing, China) and Sprague-Dawley (SD) rats were from Shanghai SLAC Laboratory Animal Co., Ltd. The mice or rats involved in this study were randomly divided into experimental groups. To establish the PCOS-like model using DHEA, 4-week-old female mice or rats were subcutaneously injected daily with DHEA (60 mg/kg body weight) for indicated consecutive days. To establish the PCOS-like model using hCG and insulin, 4-week-old female mice or rats were injected with insulin along with twice-daily injections of 0.21 IU of hCG. The dosage of insulin was gradually increased from 0.07 IU on day 1 to 0.84 IU on day 11 and maintained at 0.84 IU for the remaining days. Serum testosterone, estrous cycle, and H&E staining of ovaries were detected to evaluate PCOS-like phenotypes. To

evaluate the prevention effect of artemisinins on PCOS, mice or rats were simultaneously injected with DHEA and ATM. To evaluate the therapeutic effect of artemisinins, mice or rats were treated with ATM after establishment of PCOS-like model. To generate LONP1 overexpression mice, AAV-LONP1 were administered to mice by intraperitoneal injection at 2 to 3 weeks old. All animals were housed at $21^\circ \pm 1^\circ\text{C}$ with a humidity of $50 \pm 5\%$ in a 12-hour light/dark cycle and were fed ad libitum with standard mouse or rat feed and water throughout the experiments. All the animal studies were approved by the Animal Care and Use Committee of the Fudan University Shanghai Medical College (20210506-001) and followed the National Institutes of Health guidelines on the care and use of animals.

Clinical study

Nineteen individuals with PCOS (female, age: 27.79 ± 3.74 years, weight: 62.1 ± 8.9 kg, BMI: $23.23 \pm 2.30 \text{ kg/m}^2$) were recruited from Department of Endocrinology and Reproductive Medicine Center, Zhongshan Hospital, Fudan University for this study. Patients included in this study fulfilled the following criteria: 1) Aged 16 to 35 years (inclusive); 2) BMI between 20 and 30 kg/m^2 ; 3) No plan for pregnancy in the ensuing 6 months; 4) Meeting all the Rotterdam diagnostic criteria: a) Menstrual abnormalities: oligomenorrhea (more than 35 days between menstrual periods and less than eight menstrual bleedings in the past year) or amenorrhea (more than 90 days between two menstrual bleedings). b) Polycystic ovary appearance on ultrasonography (number of ovarian antral follicles in each ovary ≥ 12 , diameter $< 10 \text{ mm}$) (61). c) Hyperandrogenemia defined as serum testosterone $> 1.67 \text{ nmol/L}$ measured by Elecsys Testosterone II (Roche Diagnostics). The exclusion criteria were as follows: 1) Previous treatment with steroids within 3 months prior to enrolment. 2) Patients with other diseases that can cause secondary polycystic ovaries, including 21-hydroxylase deficiency, prolactinoma, hypothyroidism, Cushing's syndrome, etc. 3) Pregnancy. 4) Patients with other serious diseases involving heart, liver, kidney, or other major organs. 5) Patients with any type of cancer. All participants took oral dihydroartemisinin (Front Pharmaceutical PLC) at a dosage of 40 mg three times daily for 12 weeks. At baseline and after 12 weeks of medication, testosterone and AMH were measured, and ovarian antral follicles were evaluated by transvaginal ultrasound. The menstrual cycles were recorded for 24 weeks before the start of treatment. After completing a 12-week course of medication, participants were then followed for an extended 12-week period without medication to record menstruation. The restoration of regular menstrual cycles was defined as the

occurrence of three consecutive spontaneous bleedings lasting for 2 to 7 days, with intervals between 21 and 35 days, during the 24-week period after the initiation of dihydroartemisinin treatment. This clinical study was approved by the Ethics Committee of Zhongshan Hospital, Fudan University (B2020-115R2), and was in accordance with the Declaration of Helsinki and Good Clinical Practice. This study was registered in ClinicalTrials.gov (NCT05465135). Informed consent was obtained from all participants before enrolment.

Cell culture and treatment

To isolate theca-interstitial cells, ovaries dissected from female C57BL/6J mice (Gempharmatech Co., Ltd) or rats (Shanghai SLAC Laboratory Animal Co., Ltd) aged 4 weeks were meticulously washed and then collected in Lebovitz's L-15 medium (Gibco, Cat no. 11415-064) with 10% FBS (Gibco, Cat no. 10091-148), 100 units/ml penicillin, and 0.1 mg/ml streptomycin. Following the removal of granulosa cells, theca-interstitial cells were isolated through collagenase (4 mg/kg, Sigma, Cat no. C4-22) digestion and cultured in McCoy's 5A medium (Gibco, Cat no. 16600-082) with 10% FBS, 100 units/ml penicillin, 0.1 mg/ml streptomycin (Biological Industries, Cat no. 03-031-1B).

BeWo cells (Cat no. CL-0500) were purchased from Procell Life Science & Technology Co., Ltd and cultured in Ham's F-12K medium (Gibco, Cat no. 21127022) containing 15% FBS. HEK293T and 293A cells were purchased from China Center for Type Culture Collection (CCTCC) and cultured in Dulbecco's modified Eagle medium (DMEM; Gibco, Cat no. 11995) containing 10% FBS. Hanbio was commissioned to establish a stable expression of CYP11A1-3×Flag in HEK293T cells. The coding sequence of *Cyp11a1* was inserted into pHBLV-CMV-MCS-3×Flag-EF1-ZsGreen-T2A-PURO vectors. The recombinant lentivirus carrying the CYP11A1-3×Flag construct was produced in HEK293T cells. Subsequently, the supernatant containing the recombinant lentivirus was collected, filtered, and then introduced into a separate culture dish of HEK293T cells. CYP11A1-3×Flag expressed cells were then subjected to selection with puromycin. To generate stable HEK293T cell lines with a knockout of *Lonp1* genes, sgRNA sequence (5'-GCTGAGCGCCAG-GCACCCGG-3') targeting *Lonp1* was designed and integrated into a CRISPR/Cas9 lentivirus vector (Hanbio Biotechnology, Shanghai, China). Recombinant CRISPR/Cas9 lentivirus harboring *Lonp1* sgRNA was generated in HEK293T cells. Then HEK293T cells were infected with the recombinant lentivirus and subjected to puromycin-based selection. LONP1-deficient monoclonal cells were then isolated using limited dilution method and subjected to gene knockout validation.

Estrous cycle analysis and fertility assessment

The stage of the estrous cycle was determined by microscopic analysis of the predominant cell type in vaginal smears. For 8 consecutive days, vaginal cells were collected from the specified mice or rats by saline lavage, with daily samples obtained. The samples were subjected to Giemsa staining and visualized under a light microscopy. Briefly, the proestrus stage was typified by predominantly nucleated cells, the estrus stage exhibited cornified squamous epithelial cells, the metestrus stage was marked by a combination of cornified cells and leukocytes, and the diestrus stage showed a predominance of leukocytes. In the fertility test, females ceased receiving injections of hCG, insulin, or ATM and then mated with proven stud males. The successful mating was determined by observation of a vaginal plug on the following day. A subset of female rats was humanely euthanized and their implantation sites were examined to confirm pregnancy 10 days after successful mating. The remaining female rats were allowed to undergo natural delivery of pups. The count of pups in the first litter was quantified.

Insulin tolerance test (ITT) and glucose tolerance test (GTT)

In ITT, mice were injected intraperitoneally with recombinant human insulin (Novo Nordisk) (0.75 IU/kg body weight) after fasting for 4 hours (from 10 a.m. to 2 p.m.). Blood glucose obtained from tail bleeds was monitored at 0, 30, 60, 90, and 120 min after insulin administration using a glucometer monitor (Roche). For the GTT, mice were injected intraperitoneally with D-glucose (2 mg/g body weight) after fasting for 16 hours (from 5 p.m. to 9 a.m.), and blood glucose obtained from tail bleeds was monitored at 0, 30, 60, 90, and 120 min after administration using a glucometer monitor.

Plasmid construct and reagents

The coding sequences of mouse *Lonp1*, including WT, the catalytically inactive variant (S844A), and the GATPKD-deleted form, as well as the *C1pp* and *C1px* coding sequence, were amplified and cloned into pcdna3.1-C-Myc vectors. For the truncated *Lonp1* constructs, *Lonp1* N-domain, ATPase domain, and proteolytic domain were separately ligated with an MTS and cloned into pcdna3.1-C-Myc vectors. Mouse *Cyp11a1* coding sequence, W56 to S66 or F252 to T259 deletion form of *Cyp11a1* was amplified and cloned into pcdna3.1-C-Flag vectors.

Artemether (Cat no. JOT-10170) and artesunate (Cat no. JOT-11124) were purchased from Chengdu Pufei De Biotech Co., Ltd. DHCA was purchased from Klamar (Cat no. 16035) and MCE. Pregnenolone (Cat no. S1914), DHT (Cat no. S4757), bortezomib (Cat no. S1013), CDDO-Me (Cat no. S8078), MG132 (Cat no. S2619), and CHX (Cat no. S7418) were from Selleck.

DMSO was from Sigma (Cat no. D2650). Human insulin was from Novo Nordisk (Novolin). Elesclomol (STA-4783) was purchased from APExBIO (Cat no. A4386).

Measurement of hormones

The levels of serum total testosterone of mice or rats were measured by chemiluminescence immunoassay using Beckman Coulter UniCel DxI800 immunology analyzer. LH and FSH levels were detected using enzyme immunoassay. To detect hormone secretion in theca-interstitial cells, the cell culture supernatant was collected after a 48-hour treatment with artemisinins. After centrifugation, progesterone, 17 α -OHP, and total testosterone levels in the supernatant were measured by chemiluminescence immunoassay. Pregnenolone was measured by enzyme immunoassay (IBL International). Hormone levels in cell culture supernatant were normalized to total protein content. During these measurements, investigators remained blinded to the group allocation.

Relative quantitative proteomics analysis

LC-MS/MS-based proteomics analysis was conducted in collaboration with Shanghai Applied Protein Technology Co. Ltd. Isolated theca-interstitial cells were harvested after 5 μ M ATM treatment for 48 hours. SDS (4% SDS, 100 mM Tris-HCl, 1 mM DTT, pH 7.6) buffer was used for sample lysis and protein extraction. Protein digestion by trypsin was performed according to filter-aided sample preparation (FASP) procedure described by Matthias Mann (62). The digest peptides of each sample were desalted on C18 Cartridges [Empore SPE Cartridges C18 (standard density), bed I.D. 7 mm, volume 3 ml, Sigma], concentrated by vacuum centrifugation, and reconstituted in 40 μ l of 0.1% (v/v) formic acid. Then 100 μ g peptide mixture of each sample was labeled using TMT reagent according to the manufacturer's instructions (Thermo Scientific). Labeled peptides were fractionated by High pH Reversed-Phase Peptide Fractionation Kit (Thermo Scientific). The dried peptide mixture was reconstituted and acidified with 0.1% TFA solution and loaded onto the equilibrated, high-pH, reversed-phase fractionation spin column. Peptides were bound to the hydrophobic resin under aqueous conditions and desalted by washing the column with water by low-speed centrifugation. A step gradient of increasing acetonitrile concentrations in a volatile high-pH elution solution was then applied to the columns to elute bound peptides into 10 different fractions collected by centrifugation. The collected fractions were desalted on C18 Cartridges [Empore SPE Cartridges C18 (standard density), bed I.D. 7 mm, volume 3 ml, Sigma] and concentrated by vacuum centrifugation.

LC-MS/MS analysis was performed on a Q Exactive mass spectrometer (Thermo Scientific)

that was coupled to Easy nLC (Proxeon Biosystems, now Thermo Fisher Scientific) for 60/90 min. The peptides were loaded onto a reverse phase trap column (Thermo Scientific Acclaim PepMap100, 100 μ m² cm, nanoViper C18) connected to the C18-reversed phase analytical column (Thermo Scientific Easy Column, 10 cm long, 75 μ m inner diameter, 3 μ m resin) in buffer A (0.1% formic acid) and separated with a linear gradient of buffer B (84% acetonitrile and 0.1% formic acid) at a flow rate of 300 nl/min controlled by Intelli-Flow technology. The mass spectrometer was operated in positive ion mode. MS data were acquired using a data-dependent top 10 method dynamically choosing the most abundant precursor ions from the survey scan (300 to 1800 m/z) for HCD fragmentation. Automatic gain control (AGC) target was set to 3e6, and maximum inject time to 10 ms. Dynamic exclusion duration was 40.0 s. Survey scans were acquired at a resolution of 70,000 at m/z 200 and resolution for HCD spectra was set to 17,500 at m/z 200, and isolation width was 2 m/z. Normalized collision energy was 30 eV and the underfill ratio, which specifies the minimum percentage of the target value likely to be reached at maximum fill time, was defined as 0.1%. The instrument was run with peptide recognition mode enabled. The MS raw data for each sample were searched using the MASCOT engine (Matrix Science, London, UK; version 2.2) embedded into Proteome Discoverer 1.4 software for identification and quantitation analysis. The proteins with differential expression ($P < 0.05$, fold change > 1.2 , or fold change < 0.83) were listed in table S1.

Measurement of testosterone in the adipocyte supernatant

The stromal vascular fraction (SVF) of subcutaneous adipose tissues was isolated and subjected to adipogenic differentiation. Following differentiation, the adipocytes were treated with insulin, androstenedione (A4) or ATM for 48 hours, after which testosterone levels in the cell culture supernatant were measured. The data were normalized to total protein content.

Co-immunoprecipitation (co-IP) and IP-MS

The co-IP assay was conducted as previously described (63, 64). Briefly, HEK293T cells that stably expressed CYP11A1-3 \times Flag or control cells were lysed in co-IP lysis buffer containing 50 mM Tris-HCl (pH 7.5), 150 mM NaCl, 5% glycerol, 0.5% Triton X-100, and protease inhibitors (Roche, Cat no. 4693159001). After centrifugation, the lysates were incubated with anti-Flag beads (Smart-Lifesciences, Cat no. SA042001) for 2 hours at 4°C. Subsequently, the beads underwent four washes using the co-IP lysis buffer, and the immunoprecipitates were separated by SDS-PAGE for Western blotting. For endogenous co-IP, cells were

lysed in co-IP lysis buffer and incubated with either IgG or anti-CYP11A1 antibody (Abcam Cat no. ab175408) overnight at 4°C, followed by incubating with rProtein A beads (SmartLifesciences, Cat no. SA012005) for 2 hours. The beads were then washed with the co-IP lysis buffer and the immunoprecipitates were separated by SDS-PAGE for Western blotting.

For IP-MS analysis, HEK293T cells that stably expressed CYP11A1-3×Flag, as well as control cells, were divided into four groups as follows: control cells treated with DMSO, CYP11A1-3×Flag cells treated with DMSO, CYP11A1-3×Flag cells treated with 5 μM ATM, and CYP11A1-3×Flag cells treated with 5 μM SM934 for 24 hours. Each group of cells were lysed in co-IP lysis buffer and subjected to immunoprecipitation. The immunoprecipitates were separated by SDS-PAGE, and gels were cut into pieces for in-gel tryptic digestion. The tryptic peptides were then subjected to LC-MS/MS Analysis. The resulting MS/MS data were processed using Proteome Discoverer 1.3. Tandem mass spectra were searched against human database. Trypsin/P was specified as cleavage enzyme allowing up to two missing cleavages. Mass error was set to 10 ppm for precursor irons and 0.22 Da for fragment irons. Carbamidomethyl on Cys were specified as fixed modification and oxidation on Met was specified as variable modification. Peptide confidence was set at high, and peptide ion score was set >20. The protein identified by MS in the CYP11A1-3×Flag cells represented potential candidates for interaction. To pinpoint artemisinin-responsive interacting proteins of CYP11A1, we focused on proteins that were common between the two groups of CYP11A1-3×Flag cells treated with ATM and SM934. We excluded proteins that were detected in the CYP11A1-3×Flag cells treated with DMSO. By applying this stringent criterion, we effectively narrowed down the candidate list. The potential CYP11A1 interacting proteins in IP-MS assay were then validated using co-IP.

Western blot

Tissues and cells were lysed in lysis buffer containing 2% SDS, 50 mM Tris-HCl (pH 6.8), 10% glycerol, 0.002% bromophenol blue, PMSF, and a protease inhibitor mixture (Roche), and then subjected to protein quantification using BCA assay kit (Yeasen Biotechnology, Cat no. 20201-A). Equal amounts of protein were separated by SDS-PAGE and transferred to a polyvinylidene difluoride membrane (Millipore Corp., Bedford, MA). The membranes were blocked with 5% skimmed milk (w/v) solution in TTBS buffer for 1 hour and incubated with the indicated primary antibodies with gentle rocking overnight at 4°C. Membranes were further incubated with the corresponding HRP-conjugated secondary antibodies (Jackson ImmunoResearch) for 1 hour at room temperature. Finally, pro-

tein bands were imaged using enhanced chemiluminescence detection kit (ShareBio, Cat no. SB-WB012) and analyzed with a luminescent ImageQuant LAS 4000 image analyzer (GE Healthcare Life Sciences). Quantification of Western blot was done using ImageJ, and the values of target proteins were normalized to the loading control protein. The primary antibodies used in the current study were: CYP11A1 (Abcam Cat no. ab175408, RRID:AB_2721042), CYP17A1 (Abcam Cat no. ab125022, RRID: AB_10975095), and HSD3B2 (Abcam Cat no. ab191515) antibodies were from Abcam; LONP1 antibody (Proteintech Cat no. 15440-1-AP, RRID:AB_2137152), STAR antibody (Proteintech Cat no. 12225-1-AP, RRID:AB_2115832), rabbit polyclonal antibody for Myc tag (Proteintech Cat no. 16286-1-AP, RRID:AB_1182162) and Flag tag (Proteintech Cat no. 20543-1-AP, RRID:AB_11232216) were from Proteintech; β-actin antibody (Sigma-Aldrich Cat no. A5441, RRID:AB_476744) and mouse monoclonal antibody for Flag tag (Sigma-Aldrich Cat no. F1804, RRID:AB_262044) antibodies were from Sigma-Aldrich; mouse antibody for Myc tag (E022050-02) was from EarthOx. Peroxidase AffiniPure Goat Anti-Rabbit IgG (H+L) (Jackson ImmunoResearch Labs Cat no. 111-035-003, RRID: AB_2313567) and Peroxidase-AffiniPure Goat Anti-Mouse IgG (H+L) (Jackson ImmunoResearch Labs Cat no. 115-035-062, RRID: AB_2338504) were from Jackson ImmunoResearch Labs.

RNA isolation and quantitative PCR

Total RNA was extracted from cells and tissues using TRIzol reagent (Thermo Fisher Scientific, Cat no. 15596018). The RNA was reverse transcribed into complementary DNA using the PrimeScript RT reagent Kit with gDNA Eraser (Cat no. RR047A, Takara Bio, Otsu, Japan) according to the manufacturer's instructions. Quantitative PCR (qPCR) was conducted on a ViiA 7 instrument (Applied Biosystems) using ChamQ Universal SYBR qPCR Master Mix (Vazyme, Cat no. Q711-02) with 18S rRNA as an endogenous control. Results are presented as means and standard deviations (SD) from three independent experiments. Primers used in qPCR were listed as follows: *Cyp11a1*, AGGTCCCTCAATGAGATCCCTT and TCCCTG-TAAATGGGGCCATAC; *Cyp17a1*, GCCCAAGT-CAAAGACACCTAAT and GTACCACAGGCAGA-GAGAATAGA; *Hsd3b2*, GGTCTTTGGGGCAGA-GGATCA and GGTACTGGGTGTCAAGAATGT-CT; 18S rRNA CGGCTTACCATCCAAGGAA and GCTGGAATTACCGCGGCT.

RNA interference

RNA interference was conducted as previously described (65, 66). Theca-interstitial cells were transfected with the siRNA oligonucleotide using Lipofectamine RNAiMAX (Thermo Fisher Scientific, Cat no. 13778075) at 50% confluence. The siRNAs were generated by GenePharma

and sequences were as follows: si-*Cyp11a1*: sense, GCUUCUUUCCCAAUCCAAATT; antisense, UUUGGAUUGGGAAAGAACGCTT. si-*Lonp1*: sense, GGAAGAGACCAACAUCUUTT; antisense, AAGGAUGUUGGUUCUUCCTT. si-*Lonp1*-2: sense, GCUGCAUACAAGAACGUATT; antisense, UUACGAUCUUGUAUG-CAGCTT. Stealth siRNA negative control (siNC) duplexes with a similar GC content were used as controls.

Generation and administration of recombinant adenovirus and AAV for LONP1

Recombinant adenovirus was generated using the ViraPower Adenoviral Expression System. For LONP1 overexpression, *LONP1* coding sequence was inserted into pAd/CMV/V5-DEST vectors (Thermo Fisher Scientific, Cat no. V49320). The vector was digested with Pael to expose the viral inverted terminal repeats, and was transfected into 293A cells to produce a crude adenoviral stock. Then the recombinant adenovirus was amplified in 293A cells with the adenoviral stock and purified using adenovirus purification kits (Sartorius, Cat no. VS-AVPQ022). The purified LONP1 adenovirus was used to treat ovarian theca-interstitial cells, with LacZ adenovirus as control. AAV-LONP1 and control AAV (Serotype 9) was purchased from Genechem. To establish LONP1 overexpression in mice, AAV-LONP1 was administered to mice by intraperitoneal injection at 2-3 weeks old.

Purification of CYP11A1 and LONP1 recombinant proteins

Vectors carrying the coding sequences of *Cyp11a1* or *Lonp1*, fused with Protein A and SUMO tags, were transfected into Expi293F cells using PEI. After being cultured at 37°C for approximately 72 hours post-transfection, cells were harvested and cell pellets were lysed in a lysis buffer containing 20 mM HEPES pH 8.0, 150 mM NaCl, 10% glycerol, 0.2% CHAPS, 2 mM DTT, and protease inhibitors. After centrifugation, the supernatant was incubated with IgG resins (Cat no. SA082005, SmartLifesciences) overnight at 4°C to enrich the tagged recombinant proteins. The resins were washed with buffer containing 20 mM HEPES pH 8.0, 150 mM NaCl, 0.1% CHAPS, 10% glycerol, and 2 mM DTT. After on-column cleavage using Ulp1 for 4 hours, the immobilized proteins were eluted from the resins and concentrated for further biochemical analysis.

Protease assays in vitro

Purified recombinant LONP1 (400 ng) and CYP11A1 (400 ng) proteins were incubated in a reaction buffer (50 mM Tris-HCl [pH 8.2], 5 mM ATP, and 5 mM MgCl₂) with or without 5 μM ATM or SM934 in a total volume of 20 μl. After incubation at 37°C for specified durations, the reactions were halted by the addition of loading buffer for subsequent SDS-PAGE analysis.

The degradation of CYP11A1 was analyzed by immunoblotting using CYP11A1 antibodies.

Bio-ATS capture assay

ATS was labeled with biotin, and the product bio-ATS underwent purification through sequential washing, extraction, and column chromatography, and was then validated by H-NMR. Purified LONP1 or CYP11A1 proteins were pre-incubated with 20 μ M free ATS, ATM or SM934 for 1 hour at 4°C in the binding buffer (20 mM Tris-HCl [pH 7.5], 100 mM KCl, 0.2% Triton X-100, and protease inhibitors). Subsequently, the proteins were incubated with 2 μ M biotin-labeled ATS for 1 hour at 4°C. The bio-ATS was then captured using high capacity streptavidin-coated agarose (Thermo Fisher Scientific, Cat no. 20359) for 1 hour at 4°C, followed by three washes with the binding buffer. The agarose was then boiled in SDS-PAGE loading buffer and subjected to Western blot assay using LONP1 or CYP11A1 antibodies. To assess the competitive binding interaction between bortezomib and ATS for LONP1, LONP1 proteins were pre-incubated with 20 μ M bortezomib for 1 hour at 4°C, and followed by the capture assay.

Surface plasmon resonance (SPR) assay

SPR experiments were performed using a Biacore 8K instrument (GE Healthcare). The recombinant mouse LONP1 proteolytic domain was immobilized onto the CM5 sensor surface following the standard amine-coupling procedure according to the manufacturer's instructions. HBS-N buffer (10 mM HEPES pH 7.4 and 150 mM NaCl) supplemented with 0.05% Tween-20 was used as the running buffer for immobilization. The binding affinity assay was performed at 25°C in the buffer containing 25 mM HEPES, pH 7.4, 150 mM NaCl, 0.1% Tween 20, and 2% DMSO. The analyte was measured using a two-fold serial dilution ranging in concentrations from 25 to 0.39 μ M and injected for 120 s at a flow rate of 30 μ L/min, followed by 150 s dissociation time. Solvent correction was made with slight variations in DMSO concentration between samples; four solvent samples ranging from 1.5 to 3% DMSO were injected at the beginning and end of the analysis. SPR data for each analyte concentration were collected and fitted to a 1:1 binding kinetics model to calculate the on-rate (k_a), the off-rate (k_d), and the equilibrium dissociation constant ($K_D = k_d/k_a$) using Biacore Evaluation Software (GE Healthcare). Each experiment was performed three times.

Thermal shift assays

HEK293T cells were transfected with pcdna3.1-LONP1-Myc or pcdna3.1-CYP11A1-Flag plasmids. After 36 hours of transfection, the cells were collected, suspended in PBS and flash-frozen with liquid nitrogen. The cells under-

went lysis through three cycles of freezing and thawing. The resulting cell lysates were incubated with artemisinins for 30 min on ice, then heated at various temperature for 10 min. Next, the lysates were boiled for 10 min in loading buffer and subjected to Western blot analysis using Myc or Flag antibodies.

Molecular docking of artemisinins with LONP1

The structural model of LONP1 was obtained from the Protein Data Bank (LONP1, PDB: 6WZV). The docking simulation was processed by Schrödinger Glide v8.1 software (Schrödinger, LLC, New York, NY, USA) without constraint, where the default settings were used, and the result was visualized through PyMOL v2.5.2.

Histochemistry and immunohistochemistry

Tissues were dissected and promptly fixed in 4% paraformaldehyde at room temperature overnight. Then formaldehyde-fixed tissues were embedded in paraffin, sectioned, and subjected to staining using the H&E staining method or with the CYP11A1 antibody (Abcam Cat no. ab175408) following the standard procedures. Histochemistry and immunohistochemistry were performed by Shanghai Rui Yu biotechnology Co., Ltd. The resulting stained samples were observed with a high-quality microscope (BX53F, Olympus). During these measurements, investigators remained blinded to the group allocation.

Statistical analysis

All statistics were calculated using GraphPad Prism software. Results are presented as mean \pm SD. The two-tailed unpaired Student's *t* test was used to compare two groups with normally distributed data. The two-tailed unpaired Student's *t* test with Welch's correction was used for two groups with unequal variances. The Mann-Whitney test was used to determine significance between data without a normal distribution. To compare more than two groups, the one-way ANOVA with Bonferroni test was used to analyze normally distributed data; nonparametric statistical analysis for the data without a normal distribution was performed using the Kruskal-Wallis test with Dunn's test for multiple comparisons. A two-way ANOVA with Bonferroni post hoc multiple comparison test was used for comparison between multiple groups with two fixed factors, with $P < 0.05$ considered as statistically significant. Statistical analysis used in each panel was described in the figure legends.

REFERENCES AND NOTES

- J. A. Boyle, H. J. Teede, PCOS: Refining diagnostic features in PCOS to optimize health outcomes. *Nat. Rev. Endocrinol.* **12**, 630–631 (2016). doi: [10.1038/nrendo.2016.157](https://doi.org/10.1038/nrendo.2016.157); pmid: [2736732](https://pubmed.ncbi.nlm.nih.gov/2736732/)
- A. E. Joham et al., Polycystic ovary syndrome. *Lancet Diabetes Endocrinol.* **10**, 668–680 (2022). doi: [10.1016/S2213-8587\(22\)00163-2](https://doi.org/10.1016/S2213-8587(22)00163-2); pmid: [35934017](https://pubmed.ncbi.nlm.nih.gov/35934017/)
- H. J. Teede et al., Recommendations From the 2023 International Evidence-based Guideline for the Assessment and Management of Polycystic Ovary Syndrome. *J. Clin. Endocrinol. Metab.* **108**, 2447–2469 (2023). doi: [10.1210/clinend/dgad463](https://doi.org/10.1210/clinend/dgad463); pmid: [37580314](https://pubmed.ncbi.nlm.nih.gov/37580314/)
- K. Uluhizarci, Z. Karaca, F. Kelestir, Role of insulin and insulin resistance in androgen excess disorders. *World J. Diabetes* **12**, 616–629 (2021). doi: [10.4239/wjd.v12.5.616](https://doi.org/10.4239/wjd.v12.5.616); pmid: [33995849](https://pubmed.ncbi.nlm.nih.gov/33995849/)
- D. A. Dumesic et al., Scientific Statement on the Diagnostic Criteria, Epidemiology, Pathophysiology, and Molecular Genetics of Polycystic Ovary Syndrome. *Endocr. Rev.* **36**, 487–525 (2015). doi: [10.1210/er.2015-1018](https://doi.org/10.1210/er.2015-1018); pmid: [26426951](https://pubmed.ncbi.nlm.nih.gov/26426951/)
- C. N. Jayasena, S. Franks, The management of patients with polycystic ovary syndrome. *Nat. Rev. Endocrinol.* **10**, 624–636 (2014). doi: [10.1038/nrendo.2014.102](https://doi.org/10.1038/nrendo.2014.102); pmid: [25022814](https://pubmed.ncbi.nlm.nih.gov/25022814/)
- M. O. Goodarzi, D. A. Dumesic, G. Chazenbalk, R. Azziz, Polycystic ovary syndrome: Etiology, pathogenesis and diagnosis. *Nat. Rev. Endocrinol.* **7**, 219–231 (2011). doi: [10.1038/nrendo.2010.217](https://doi.org/10.1038/nrendo.2010.217); pmid: [21263450](https://pubmed.ncbi.nlm.nih.gov/21263450/)
- R. L. Rosenfield, D. A. Ehrmann, The Pathogenesis of Polycystic Ovary Syndrome (PCOS): The Hypothesis of PCOS as Functional Ovarian Hyperandrogenism Revisited. *Endocr. Rev.* **37**, 467–520 (2016). doi: [10.1210/er.2015-1104](https://doi.org/10.1210/er.2015-1104); pmid: [27459230](https://pubmed.ncbi.nlm.nih.gov/27459230/)
- P. Kempegowda, E. Melson, K. N. Manolopoulos, W. Arlt, M. W. O'Reilly, Implicating androgen excess in propagating metabolic disease in polycystic ovary syndrome. *Ther. Adv. Endocrinol. Metab.* **11**, 204201820934319 (2020). doi: [10.1177/204201820934319](https://doi.org/10.1177/204201820934319); pmid: [32637065](https://pubmed.ncbi.nlm.nih.gov/32637065/)
- S. Risal et al., Prenatal androgen exposure and transgenerational susceptibility to polycystic ovary syndrome. *Nat. Med.* **25**, 1894–1904 (2019). doi: [10.1038/s41591-019-0666-1](https://doi.org/10.1038/s41591-019-0666-1); pmid: [31792459](https://pubmed.ncbi.nlm.nih.gov/31792459/)
- W. L. Miller, R. J. Auchus, The molecular biology, biochemistry, and physiology of human steroidogenesis and its disorders. *Endocr. Rev.* **32**, 81–151 (2011). doi: [10.1210/er.2010-0013](https://doi.org/10.1210/er.2010-0013); pmid: [21051590](https://pubmed.ncbi.nlm.nih.gov/21051590/)
- Y. Chien, K. Rosal, B. C. Chung, Function of CYP11A1 in the mitochondria. *Mol. Cell. Endocrinol.* **441**, 55–61 (2017). doi: [10.1016/j.mce.2016.10.030](https://doi.org/10.1016/j.mce.2016.10.030); pmid: [27815210](https://pubmed.ncbi.nlm.nih.gov/27815210/)
- V. L. Nelson, R. S. Legro, J. F. Strauss3rd, J. M. McAllister, Augmented androgen production is a stable steroidogenic phenotype of propagated theca cells from polycystic ovaries. *Mol. Endocrinol.* **13**, 946–957 (1999). doi: [10.1210/mend.13.6.0311](https://doi.org/10.1210/mend.13.6.0311); pmid: [10379893](https://pubmed.ncbi.nlm.nih.gov/10379893/)
- V. L. Nelson et al., The biochemical basis for increased testosterone production in theca cells propagated from patients with polycystic ovary syndrome. *J. Clin. Endocrinol. Metab.* **86**, 5925–5933 (2001). doi: [10.1210/jcem.86.12.8088](https://doi.org/10.1210/jcem.86.12.8088); pmid: [11739466](https://pubmed.ncbi.nlm.nih.gov/11739466/)
- J. K. Wickenheisser et al., Cholesterol side-chain cleavage gene expression in theca cells: Augmented transcriptional regulation and mRNA stability in polycystic ovary syndrome. *PLOS ONE* **7**, e48963 (2012). doi: [10.1371/journal.pone.0048963](https://doi.org/10.1371/journal.pone.0048963); pmid: [23155436](https://pubmed.ncbi.nlm.nih.gov/23155436/)
- J. K. Wickenheisser, V. L. Nelson-DeGrave, J. M. McAllister, Human ovarian theca cells in culture. *Trends Endocrinol. Metab.* **17**, 65–71 (2006). doi: [10.1016/j.tem.2006.01.003](https://doi.org/10.1016/j.tem.2006.01.003); pmid: [16460956](https://pubmed.ncbi.nlm.nih.gov/16460956/)
- K. M. Hoeger, A. Dokras, T. Piltonen, Update on PCOS: Consequences, Challenges, and Guiding Treatment. *J. Clin. Endocrinol. Metab.* **106**, e1071–e1083 (2021). doi: [10.1210/cinem/dgaa839](https://doi.org/10.1210/cinem/dgaa839); pmid: [33211867](https://pubmed.ncbi.nlm.nih.gov/33211867/)
- Y. Tu, The discovery of artemisinin (qinghaosu) and gifts from Chinese medicine. *Nat. Med.* **17**, 1217–1220 (2011). doi: [10.1038/nm.2471](https://doi.org/10.1038/nm.2471); pmid: [21989013](https://pubmed.ncbi.nlm.nih.gov/21989013/)
- P. Lu et al., Artemisinin derivatives prevent obesity by inducing browning of WAT and enhancing BAT function. *Cell Res.* **26**, 1169–1172 (2016). doi: [10.1038/cr.2016.108](https://doi.org/10.1038/cr.2016.108); pmid: [27633061](https://pubmed.ncbi.nlm.nih.gov/27633061/)
- N. E. Baskind, A. H. Balen, Hypothalamic-pituitary, ovarian and adrenal contributions to polycystic ovary syndrome. *Best Pract. Res. Clin. Obstet. Gynaecol.* **37**, 80–97 (2016). doi: [10.1016/j.bpobgyn.2016.03.005](https://doi.org/10.1016/j.bpobgyn.2016.03.005); pmid: [27137106](https://pubmed.ncbi.nlm.nih.gov/27137106/)
- L. F. Hou et al., SM934, a water-soluble derivative of artemisinin, exerts immunosuppressive functions in vitro and in vivo. *Int. Immunopharmacol.* **9**, 1509–1517 (2009). doi: [10.1016/j.intimp.2009.09.003](https://doi.org/10.1016/j.intimp.2009.09.003); pmid: [19772931](https://pubmed.ncbi.nlm.nih.gov/19772931/)
- M. W. O'Reilly et al., AKR1C-Mediated Adipose Androgen Generation Drives Lipotoxicity in Women With Polycystic Ovary Syndrome. *J. Clin. Endocrinol. Metab.* **102**, 3327–3339 (2017). doi: [10.1210/jc.2017-00947](https://doi.org/10.1210/jc.2017-00947); pmid: [28645211](https://pubmed.ncbi.nlm.nih.gov/28645211/)
- M. Quinkler et al., Androgen generation in adipose tissue in women with simple obesity—A site-specific role for 17beta-hydroxysteroid dehydrogenase type 5. *J. Endocrinol.*

- 183, 331–342 (2004). doi: [10.1677/joe.1.05762](https://doi.org/10.1677/joe.1.05762); pmid: [15531721](https://pubmed.ncbi.nlm.nih.gov/15531721/)
24. D. M. Stocco, StAR protein and the regulation of steroid hormone biosynthesis. *Annu. Rev. Physiol.* **63**, 193–213 (2001). doi: [10.1146/annurev.physiol.63.1193](https://doi.org/10.1146/annurev.physiol.63.1193); pmid: [1181954](https://pubmed.ncbi.nlm.nih.gov/1181954/)
25. S. Shen et al., The potential of artemisinins against obesity agents via modulating the immune system. *Pharmacol. Ther.* **216**, 107696 (2020). doi: [10.1016/j.pharmthera.2020.107696](https://doi.org/10.1016/j.pharmthera.2020.107696); pmid: [33022301](https://pubmed.ncbi.nlm.nih.gov/33022301/)
26. D. A. Bota, K. J. Davies, Mitochondrial Lon protease in human disease and aging: Including an etiologic classification of Lon-related diseases and disorders. *Free Radic. Biol. Med.* **100**, 188–198 (2016). doi: [10.1016/j.freeradbiomed.2016.06.031](https://doi.org/10.1016/j.freeradbiomed.2016.06.031); pmid: [27387767](https://pubmed.ncbi.nlm.nih.gov/27387767/)
27. M. G. Hanna4th et al., TGF facilitates outer coat disassembly on COPII transport carriers to promote tethering and fusion with ER-Golgi intermediate compartments. *Proc. Natl. Acad. Sci. U.S.A.* **114**, E7707–E7716 (2017). doi: [10.1073/pnas.1709120114](https://doi.org/10.1073/pnas.1709120114); pmid: [28851831](https://pubmed.ncbi.nlm.nih.gov/28851831/)
28. S. L. Schreiber, The Rise of Molecular Glues. *Cell* **184**, 3–9 (2021). doi: [10.1016/j.cell.2020.12.020](https://doi.org/10.1016/j.cell.2020.12.020); pmid: [33417864](https://pubmed.ncbi.nlm.nih.gov/33417864/)
29. Z. Granot et al., Turnover of mitochondrial steroidogenic acute regulatory (StAR) protein by Lon protease: The unexpected effect of proteasome inhibitors. *Mol. Endocrinol.* **21**, 2164–2177 (2007). doi: [10.1210/me.2005-0458](https://doi.org/10.1210/me.2005-0458); pmid: [17579211](https://pubmed.ncbi.nlm.nih.gov/17579211/)
30. S. H. Bernstein et al., The mitochondrial ATP-dependent Lon protease: A novel target in lymphoma death mediated by the synthetic triterpenoid CDDO and its derivatives. *Blood* **119**, 3321–3329 (2012). doi: [10.1182/blood-2011-02-340075](https://doi.org/10.1182/blood-2011-02-340075); pmid: [22323447](https://pubmed.ncbi.nlm.nih.gov/22323447/)
31. O. Zurita Rendón, E. A. Shoubridge, LONP1 Is Required for Maturation of a Subset of Mitochondrial Proteins, and Its Loss Elicits an Integrated Stress Response. *Mol. Cell. Biol.* **38**, e00412-17 (2018). doi: [10.1128/MCB.00412-17](https://doi.org/10.1128/MCB.00412-17); pmid: [30061372](https://pubmed.ncbi.nlm.nih.gov/30061372/)
32. T. Liu et al., DNA and RNA binding by the mitochondrial Lon protease is regulated by nucleotide and protein substrate. *J. Biol. Chem.* **279**, 13902–13910 (2004). doi: [10.1074/jbc.M309642200](https://doi.org/10.1074/jbc.M309642200); pmid: [1473929](https://pubmed.ncbi.nlm.nih.gov/15473929/)
33. P. J. Thul et al., A subcellular map of the human proteome. *Science* **356**, eaal3321 (2017). doi: [10.1126/science.aal3321](https://doi.org/10.1126/science.aal3321); pmid: [28495876](https://pubmed.ncbi.nlm.nih.gov/28495876/)
34. J. Song, J. M. Herrmann, T. Becker, Quality control of the mitochondrial proteome. *Nat. Rev. Mol. Cell Biol.* **22**, 54–70 (2021). doi: [10.1038/s41580-020-00300-2](https://doi.org/10.1038/s41580-020-00300-2); pmid: [33093673](https://pubmed.ncbi.nlm.nih.gov/33093673/)
35. J. R. Wood et al., Valproate-induced alterations in human theca cell gene expression: Clues to the association between valproate use and metabolic side effects. *Physiol. Genomics* **20**, 233–243 (2005). doi: [10.1152/physiogenomics.00193.2004](https://doi.org/10.1152/physiogenomics.00193.2004); pmid: [15598877](https://pubmed.ncbi.nlm.nih.gov/15598877/)
36. S. Paul, S. Kundu, K. Pramanick, A. Bandyopadhyay, D. Mukherjee, Regulation of ovarian steroidogenesis in vitro by gonadotropin in common carp Cyprinus carpio: Interaction between calcium- and adenylate cyclase-dependent pathways and involvement of ERK signaling cascade. *J. Mol. Endocrinol.* **45**, 207–218 (2010). doi: [10.1677/JME-10-0061](https://doi.org/10.1677/JME-10-0061); pmid: [20668068](https://pubmed.ncbi.nlm.nih.gov/20668068/)
37. L. J. Kingsley et al., Structure-Based Design of Selective LONP1 Inhibitors for Probing *In Vitro* Biology. *J. Med. Chem.* **64**, 4857–4869 (2021). doi: [10.1021/acs.jmedchem.0c02152](https://doi.org/10.1021/acs.jmedchem.0c02152); pmid: [33821636](https://pubmed.ncbi.nlm.nih.gov/33821636/)
38. C. R. Harding et al., Genetic screens reveal a central role for heme metabolism in artemisinin susceptibility. *Nat. Commun.* **11**, 4813 (2020). doi: [10.1038/s41467-020-18624-0](https://doi.org/10.1038/s41467-020-18624-0); pmid: [32968076](https://pubmed.ncbi.nlm.nih.gov/32968076/)
39. J. Wang et al., Haem-activated promiscuous targeting of artemisinin in Plasmodium falciparum. *Nat. Commun.* **6**, 10111 (2015). doi: [10.1038/ncomms10111](https://doi.org/10.1038/ncomms10111); pmid: [26694030](https://pubmed.ncbi.nlm.nih.gov/26694030/)
40. U. Eckstein-Ludwig et al., Artemisinins target the SERCA of Plasmodium falciparum. *Nature* **424**, 957–961 (2003). doi: [10.1038/nature01813](https://doi.org/10.1038/nature01813); pmid: [12931192](https://pubmed.ncbi.nlm.nih.gov/12931192/)
41. A. Mbengue et al., A molecular mechanism of artemisinin resistance in *Plasmodium falciparum* malaria. *Nature* **520**, 683–687 (2015). doi: [10.1038/nature14412](https://doi.org/10.1038/nature14412); pmid: [25874676](https://pubmed.ncbi.nlm.nih.gov/25874676/)
42. J. Li et al., Artemisinins Target GABA_A Receptor Signaling and Impair α Cell Identity. *Cell* **168**, 86–100.e15 (2017). doi: [10.1016/j.cell.2016.11.010](https://doi.org/10.1016/j.cell.2016.11.010); pmid: [27916275](https://pubmed.ncbi.nlm.nih.gov/27916275/)
43. X. Yuan et al., Brown adipose tissue transplantation ameliorates polycystic ovary syndrome. *Proc. Natl. Acad. Sci. U.S.A.* **113**, 2708–2713 (2016). doi: [10.1073/pnas.1523236113](https://doi.org/10.1073/pnas.1523236113); pmid: [26903641](https://pubmed.ncbi.nlm.nih.gov/26903641/)
44. X. Qi et al., Gut microbiota-bile acid-interleukin-22 axis orchestrates polycystic ovary syndrome. *Nat. Med.* **25**, 1225–1233 (2019). doi: [10.1038/s41591-019-0509-0](https://doi.org/10.1038/s41591-019-0509-0); pmid: [31332392](https://pubmed.ncbi.nlm.nih.gov/31332392/)
45. J. A. Visser, The importance of metabolic dysfunction in polycystic ovary syndrome. *Nat. Rev. Endocrinol.* **17**, 77–78 (2021). doi: [10.1038/s41574-020-00456-z](https://doi.org/10.1038/s41574-020-00456-z); pmid: [33318648](https://pubmed.ncbi.nlm.nih.gov/33318648/)
46. W. Abdrabou et al., Metabolome modulation of the host adaptive immunity in human malaria. *Nat. Metab.* **3**, 1001–1016 (2021). doi: [10.1038/s42255-021-00404-9](https://doi.org/10.1038/s42255-021-00404-9); pmid: [34113019](https://pubmed.ncbi.nlm.nih.gov/34113019/)
47. R. Jambou et al., Resistance of *Plasmodium falciparum* field isolates to in-vitro artemether and point mutations of the SERCA-type PfATPase6. *Lancet* **366**, 1960–1963 (2005). doi: [10.1016/S0140-6736\(05\)67787-2](https://doi.org/10.1016/S0140-6736(05)67787-2); pmid: [16325698](https://pubmed.ncbi.nlm.nih.gov/16325698/)
48. H. Noedl et al., Evidence of artemisinin-resistant malaria in western Cambodia. *N. Engl. J. Med.* **359**, 2619–2620 (2008). doi: [10.1056/NEJM0805011](https://doi.org/10.1056/NEJM0805011); pmid: [19064625](https://pubmed.ncbi.nlm.nih.gov/19064625/)
49. L. Corrie et al., Recent updates on animal models for understanding the etiopathogenesis of polycystic ovarian syndrome. *Life Sci.* **280**, 119753 (2021). doi: [10.1016/j.lfs.2021.119753](https://doi.org/10.1016/j.lfs.2021.119753); pmid: [34171379](https://pubmed.ncbi.nlm.nih.gov/34171379/)
50. D. A. Bota, K. J. Davies, Lon protease preferentially degrades oxidized mitochondrial aconitase by an ATP-stimulated mechanism. *Nat. Cell Biol.* **4**, 674–680 (2002). doi: [10.1038/ncb836](https://doi.org/10.1038/ncb836); pmid: [12198491](https://pubmed.ncbi.nlm.nih.gov/12198491/)
51. B. Lu et al., Phosphorylation of human TFAM in mitochondria impairs DNA binding and promotes degradation by the AAA+ Lon protease. *Mol. Cell* **49**, 121–132 (2013). doi: [10.1016/j.molcel.2012.10.023](https://doi.org/10.1016/j.molcel.2012.10.023); pmid: [23201127](https://pubmed.ncbi.nlm.nih.gov/23201127/)
52. C. S. Shin et al., LONP1 and mtHSP70 cooperate to promote mitochondrial protein folding. *Nat. Commun.* **12**, 265 (2021). doi: [10.1038/s41467-020-20597-z](https://doi.org/10.1038/s41467-020-20597-z); pmid: [33431889](https://pubmed.ncbi.nlm.nih.gov/33431889/)
53. P. M. Quirós, T. Langer, C. López-Otín, New roles for mitochondrial proteases in health, ageing and disease. *Nat. Rev. Mol. Cell Biol.* **16**, 345–359 (2015). doi: [10.1038/nrm3984](https://doi.org/10.1038/nrm3984); pmid: [25970558](https://pubmed.ncbi.nlm.nih.gov/25970558/)
54. A. Bahat et al., StAR enhances transcription of genes encoding the mitochondrial proteases involved in its own degradation. *Mol. Endocrinol.* **28**, 208–224 (2014). doi: [10.1210/me.2013-1275](https://doi.org/10.1210/me.2013-1275); pmid: [24422629](https://pubmed.ncbi.nlm.nih.gov/24422629/)
55. A. Laleve et al., Artemisinin and its derivatives target mitochondrial c-type cytochromes in yeast and human cells. *Biochim. Biophys. Acta Mol. Cell Res.* **1867**, 118661 (2020). doi: [10.1016/j.bbamcr.2020.118661](https://doi.org/10.1016/j.bbamcr.2020.118661); pmid: [31987792](https://pubmed.ncbi.nlm.nih.gov/31987792/)
56. D. A. Bota, H. Van Remmen, K. J. Davies, Modulation of Lon protease activity and aconitase turnover during aging and oxidative stress. *FEBS Lett.* **532**, 103–106 (2002). doi: [10.1016/S0014-5793\(02\)03638-4](https://doi.org/10.1016/S0014-5793(02)03638-4); pmid: [12459471](https://pubmed.ncbi.nlm.nih.gov/12459471/)
57. Z. Xu et al., Disuse-associated loss of the protease LONP1 in muscle impairs mitochondrial function and causes reduced skeletal muscle mass and strength. *Nat. Commun.* **13**, 894 (2022). doi: [10.1038/s41467-022-28557-5](https://doi.org/10.1038/s41467-022-28557-5); pmid: [35173176](https://pubmed.ncbi.nlm.nih.gov/35173176/)
58. Q. Yang et al., LONP-1 and ATFS-1 sustain deleterious heteroplasmy by promoting mtDNA replication in dysfunctional mitochondria. *Nat. Cell Biol.* **24**, 181–193 (2022). doi: [10.1038/s41556-021-00840-5](https://doi.org/10.1038/s41556-021-00840-5); pmid: [35165413](https://pubmed.ncbi.nlm.nih.gov/35165413/)
59. X. Sheng et al., The mitochondrial protease LONP1 maintains oocyte development and survival by suppressing nuclear translocation of AIFM1 in mammals. *EBioMedicine* **75**, 103790 (2022). doi: [10.1016/j.ebiom.2021.103790](https://doi.org/10.1016/j.ebiom.2021.103790); pmid: [34974310](https://pubmed.ncbi.nlm.nih.gov/34974310/)
60. Z. Kozicka, N. H. Thomä, Haven't got a glue: Protein surface variation for the design of molecular glue degraders. *Cell Chem. Biol.* **28**, 1032–1047 (2021). doi: [10.1016/j.chembiol.2021.04.009](https://doi.org/10.1016/j.chembiol.2021.04.009); pmid: [33930325](https://pubmed.ncbi.nlm.nih.gov/33930325/)
61. Rotterdam ESHRE/ASRM-Sponsored PCOS consensus workshop group, Revised 2003 consensus on diagnostic criteria and long-term health risks related to polycystic ovary syndrome (PCOS). *Hum. Reprod.* **19**, 41–47 (2004). doi: [10.1093/humrep/deh098](https://doi.org/10.1093/humrep/deh098); pmid: [14688154](https://pubmed.ncbi.nlm.nih.gov/14688154/)
62. J. R. Wiśniewski, A. Zougman, N. Nagaraj, M. Mann, Universal sample preparation method for proteome analysis. *Nat. Methods* **6**, 359–362 (2009). doi: [10.1038/nmeth.1322](https://doi.org/10.1038/nmeth.1322); pmid: [19377485](https://pubmed.ncbi.nlm.nih.gov/19377485/)
63. Y. Liu et al., Hepatic Small Ubiquitin-Related Modifier (SUMO)-Specific Protease 2 Controls Systemic Metabolism Through SUMOylation-Dependent Regulation of Liver-Adipose Tissue Crosstalk. *Hepatology* **74**, 1864–1883 (2021). doi: [10.1002/hep.31881](https://doi.org/10.1002/hep.31881); pmid: [33934381](https://pubmed.ncbi.nlm.nih.gov/33934381/)
64. X. Dou et al., The protease SENP2 controls hepatic gluconeogenesis by regulating the SUMOylation of the fuel sensor AMPKα. *J. Biol. Chem.* **298**, 101544 (2022). doi: [10.1016/j.jbc.2021.101544](https://doi.org/10.1016/j.jbc.2021.101544); pmid: [34971706](https://pubmed.ncbi.nlm.nih.gov/34971706/)
65. M. Ding et al., CHCHD10 Modulates Thermogenesis of Adipocytes by Regulating Lipolysis. *Diabetes* **71**, 1862–1879 (2022). doi: [10.2337/db21-0999](https://doi.org/10.2337/db21-0999); pmid: [35709007](https://pubmed.ncbi.nlm.nih.gov/35709007/)
66. M. Ding et al., CLCF1 signaling restrains thermogenesis and disrupts metabolic homeostasis by inhibiting mitochondrial biogenesis in brown adipocytes. *Proc. Natl. Acad. Sci. U.S.A.* **120**, e230571720 (2023). doi: [10.1073/pnas.2305717120](https://doi.org/10.1073/pnas.2305717120); pmid: [37549287](https://pubmed.ncbi.nlm.nih.gov/37549287/)

ACKNOWLEDGMENTS

We are grateful to J.-P. Zuo from the Shanghai Institute of Materia Medica for providing the SM934 agent and to Y.-F. Ke at Fudan University for assisting in animal model experiments. **Funding:** This research was supported by National Key R&D Program of China grant 2018YFA0800400 (Q.-Q.T.), National Natural Science Foundation of China grants 82170884, 81970744, and 81601251 (Y.L.), National Natural Science Foundation of China grant 81730021 (Q.-Q.T.), Shanghai Rising-Star Program grant 22QA140210 (Y.L.), and National Key R&D Program of China grant 2021YFC2700400 (X.-Y.L.), and by scientific research projects of the Shanghai Health Commission grant 20204Y0116 (Y.L.). **Author contributions:** Conceptualization: Q.-Q.T. and Y.L.; Investigation: Y.L., J.-J.J., S.-Y.D., L.-S.M., J.-J.F., J.-C.H., Y.Y., M.D., W.-Y.Z., Q.-H.Y., Y.-F.X., H.-Y.X., Y.-J.S., S.-W.Q., Y.T., and W.L.; Funding acquisition: Y.L., Q.-Q.T., and X.-Y.L.; Project administration: Q.-Q.T., Y.L., X.-Y.D., X.-Y.L., Y.-J.D., and C.-J.X.; Supervision: Q.-Q.T. and Y.L.; Writing – original draft: Y.L.; Writing – review and editing: Y.L. and Q.-Q.T. **Competing interests:** Q.-Q.T., Y.L., C.-J.X., and S.-Y.D. are inventors on a patent application (202110938195.4) titled "The application of artemisinin analogues in the preparation of drugs for treating diseases related to hyperandrogenemia." The other authors declare that they have no competing interests. **Data and materials availability:** All data are available in the main text or the supplementary materials. **License information:** Copyright © 2024 the authors, some rights reserved; exclusive licensee American Association for the Advancement of Science. No claim to original US government works. <https://www.science.org/about/science-licenses-journal-article-reuse>

SUPPLEMENTARY MATERIALS

science.org/doi/10.1126/science.adk5382

Figs. S1 to S14

Table S1

MDAR Reproducibility Checklist

Submitted 29 August 2023; accepted 19 April 2024

10.1126/science.adk5382